6.9 APPENDICES

Appendix	Description
6.9.1	FISSILE CONTENT MODELS
6.9.2	HAC PACKAGE MODEL
6.9.3	PACKAGE MATERIAL COMPOSITIONS
6.9.4	QUALIFICATION OF A NEUTRON ABSORBER MATERIAL FOR THE ES-3100
6.9.5	MISCELLANEOUS INFORMATION AND DATA
6.9.6	ABRIDGED SUMMARY TABLES OF CRITICALITY CALCULATION RESULTS
6.9.7	INPUT LISTINGS OF ES-3100 CALCULATION MODELS FOR SELECT CASES

Appendix 6.9.1

FISSILE CONTENT MODELS

Appendix 6.9.1

FISSILE CONTENT MODELS

Figure 6.9.1-1 depicts the wire-mesh view of the 3.24-in.-diam highly enriched uranium (HEU) cylindrical content configuration inside the containment vessel. The interstitial water has been removed for illustration purposes. As can be seen from Fig. 6.9.1-1, the cylindrical content model contains one cylinder per convenience can and 1.4-in.-thick 277-4 canned spacers between the can locations. Cylinders are at the maximum diameter that will fit through the opening of a press-fit lid type convenience can. The cylindrical content shown is at the maximum mass loading; the height of the cylinders may change depending upon the mass loading.

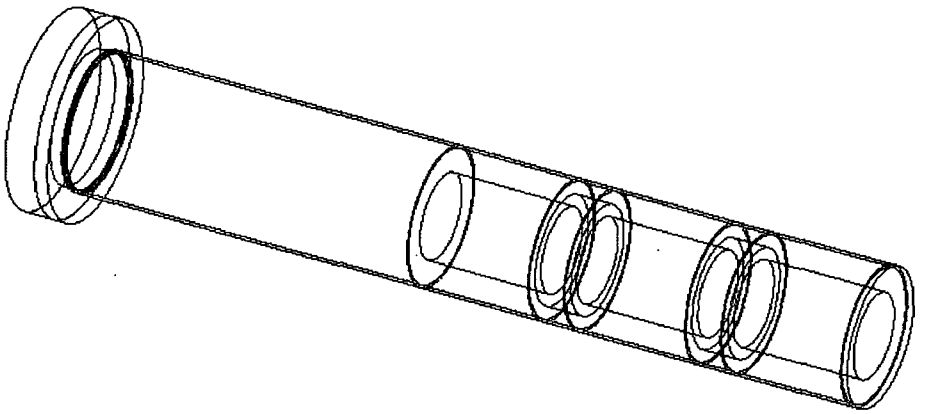

Fig. 6.9.1-1. Containment vessel containing 3.24-in.-diam cylinders and 1.4-in.-thick 277-4 canned spacers.

Figure 6.9.1-2 depicts the wire-mesh view of the 4.25-in.-diam HEU cylindrical content configuration inside the containment vessel. The interstitial water has been removed for illustration purposes. As can be seen from Fig. 6.9.1-2, the cylindrical content model contains one cylinder per convenience can and 1.4-in.-thick 277-4 canned spacers between the can locations. Cylinders are at the maximum diameter that will fit through the opening of a crimp-seal lid type convenience can. The cylindrical content shown is at the maximum mass loading; the height of the cylinders may change depending upon the mass loading.

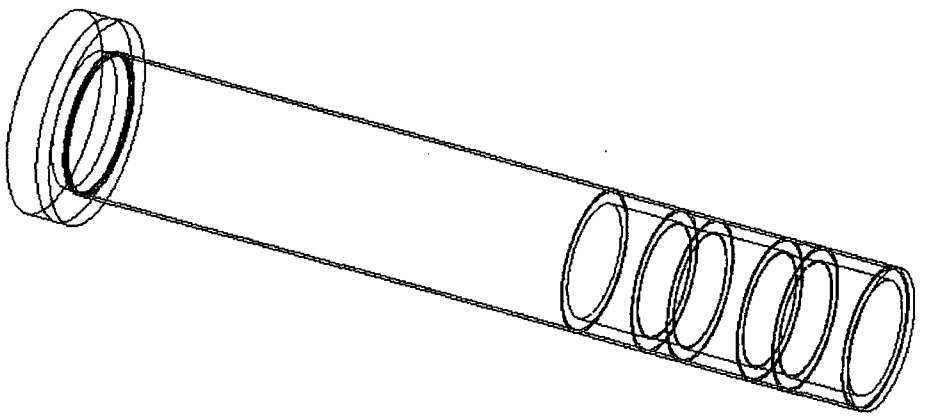

Fig. 6.9.1-2. Containment vessel containing 4.25-in.-diam cylinders and 1.4-in.-thick 277-4 canned spacers.

Figure 6.9.1-3 depicts the wire-mesh view of the 2.29-in.-square HEU bar content configuration inside the containment vessel. The interstitial water inside the containment vessel has been removed for illustration purposes. The square bar content model contains one bar per convenience can and 1.4-in.-thick 277-4 canned spacers between the can locations. The 2.29-in.-square bar is the largest size that will fit through the 3.24-in.-diam opening of a press-fit lid type convenience can. Similar to the cylindrical model, the height of the square bar is dependent upon the HEU mass.

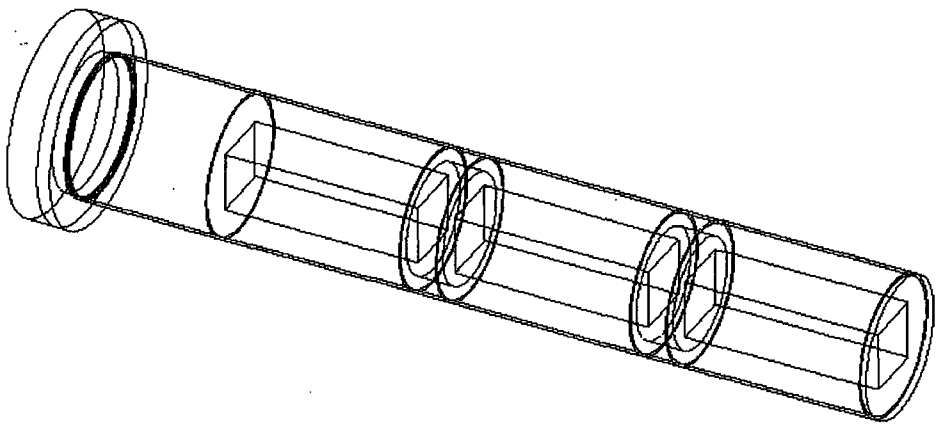

Fig. 6.9.1-3. Containment vessel containing 2.29-in.-square bars and 1.4-in.-thick 277-4 canned spacers.

Figure 6.9.1-4 depicts the wire-mesh view of a pentagonal ring configuration of the 1.5-in.-diam × 2.0-in.-tall slugs inside the containment vessel. The axial centerline of each slug is located 1.27598 in. from the origin of the pentagon such that a tight fitting configuration of slugs is modeled (i.e., there are no gaps between adjacent slugs). The slug content model contains two rings of the 1.5-in.-diam × 2.0-in.-tall slugs per convenience can and the 277-4 canned spacers between the convenience cans locations. The interstitial water inside the containment vessel has been removed for illustration purposes. Figure 6.9.1-4b depicts typical slug configurations that were evaluated.

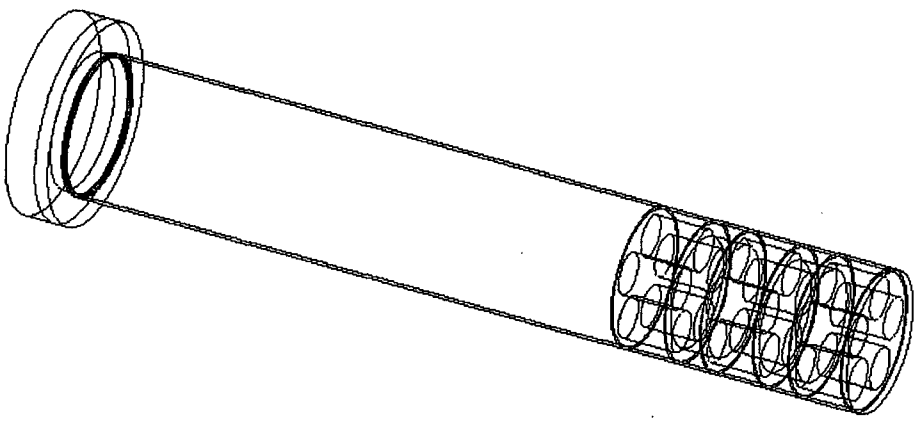

Fig. 6.9.1-4. Containment vessel containing the 1.5-in.-diam × 2.0-in.-tall slugs in a pentagonal ring configuration with 0.0-cm spacing between slugs and 1.4-in.-thick 277-4 canned spacers.

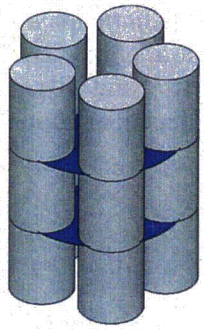

cvcr5est11_1_1
18,287 g ^{235}U
no canned spacers

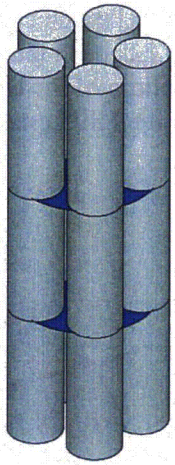

cvcr5est11_1_2
36,573 g ^{235}U
no canned spacers

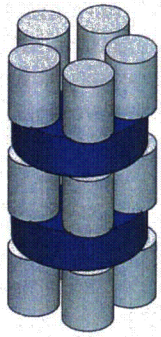

cvcr5est11_2_1
18,287 g ^{235}U
canned spacers

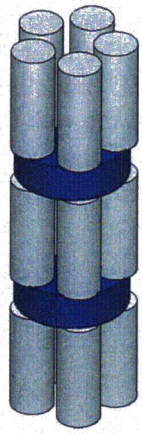

cvcr5est11_2_2
36,573 g ^{235}U
canned spacers

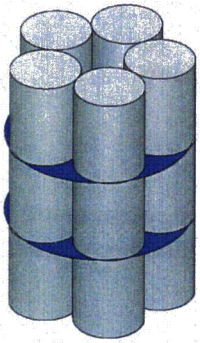

cvcr5st11_1_1
18,287 g ^{235}U
no canned spacers

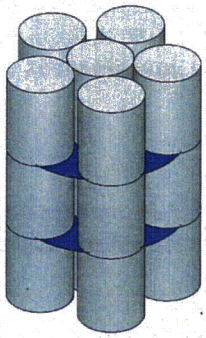

cvcr6e0t11_1_1
21,944 g ^{235}U
no canned spacers

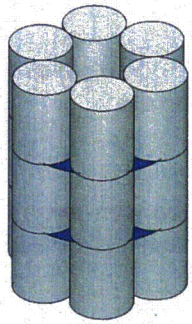

cvcr6st11_1_1
21,944 g ^{235}U
no canned spacers

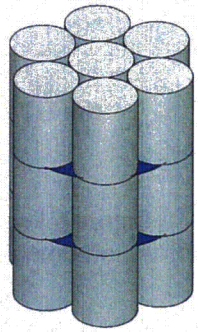

cvcr70st11_1_1
25,601 g ^{235}U
no canned spacers

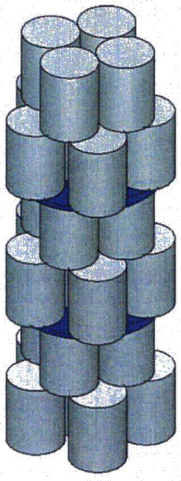

cvcr6e4t11_1_1
36,573 g ^{235}U
no canned spacers

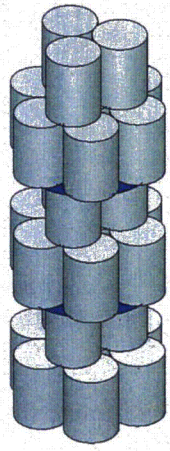

cvcr73t11_1_1
36,573 g ^{235}U
no canned spacers

Fig. 6.9.1-4b. Typical slug configurations. Blue marker depicted for configurations without 1.4-in.-thick 277-4 canned spacers.

Figure 6.9.1-5 depicts the wire-mesh view of the HEU oxide content inside the containment vessel. The interstitial water inside the containment vessel has been removed for illustration purposes. The HEU oxide mixture at bulk density is located at the bottom of the containment vessel and fills the space to the wall of the containment vessel. The height of the HEU oxide mixture is dependant upon the mass loading.

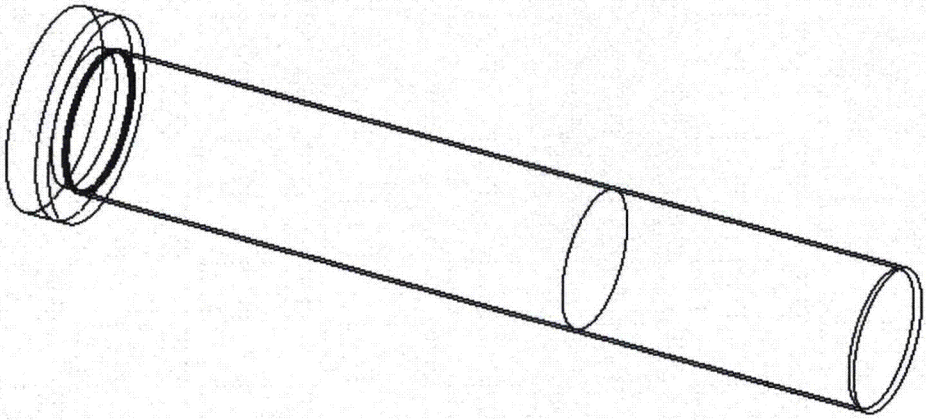

Fig. 6.9.1-5. Wire-mesh view of the containment vessel containing the HEU oxide mixture.

Figure 6.9.1-6 depicts the wire-mesh view of the UNH crystal content inside the containment vessel. A solution of UNH crystals dissolved in water fills the entire volume of the containment vessel.

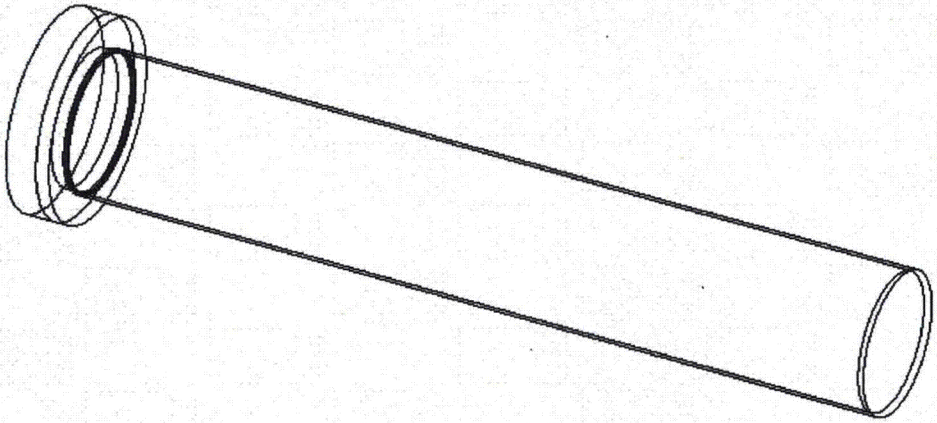

Fig. 6.9.1-6. Wire-mesh view of the containment vessel containing the UNH crystal mixture.

Wire-frame figures for the HEU broken metal models are presented in Appendix 6.9.3 (Figs. 6.9.3.1-4, 6.9.3.1-4b, 6.9.3.1-5, and 6.9.3.1-6).

Appendix 6.9.2

HAC PACKAGE MODEL

Appendix 6.9.2

HAC PACKAGE MODEL

6.9.2.1 PREDICTION OF HAC DAMAGE IN THE ES-3100 PACKAGE

Finite element analysis of an ES-3100 package under Hypothetical Accident Conditions (HAC) is used to predict the deformed outer diameters of the drum at node points along the vertical axis of an upright package. Selected node points are designated in a downward direction from the top of the drum as "UR," "MUR," "MR," "MLR," and "LR." Table 6.9.2.1-1 lists diameters at the five node points measured along the 90–270° and 0–180° axes. These dimensions represent major and minor axes at each deformation point on the assumption that the drum cross section is ellipsoidal. A corresponding equivalent circular diameter is also listed for each node point in Table 6.9.2.1-1.

A set of KENO V.a calculation models based on reduced package diameters at the "MR," "MLR," and "LR" deformation points are derived from the Normal Conditions of Transport (NCT) geometry model. These geometry models are evaluated for the purpose of establishing a bounding geometry model for representing the ES-3100 package under HAC. The primary changes made to the KENO V.a geometry input statements in the NCT model are reductions in the drum's radii. The change to the drum's inner radius also affects the outer radius of both the angle iron and the Kaolite located inside the containment vessel outer liner. The volume fractions for these materials are adjusted in the KENO V.a calculation models so that material masses of the affected package components are conserved. Table 6.9.2.1-2 provides data for transforming the KENO V.a calculation model from an NCT model into an HAC model.

6.9.2.2 CRITICALITY CALCULATIONS

Sets of criticality calculations are performed for the "MR," "MLR," and "LR" models at five different package water contents over the range of HAC. The five package water contents of the void spaces external to the containment vessel and the interstitial space between drums are as follows: 1e-20 spg water, 1e-04 spg water, 0.1 spg water, 0.3 spg water, and 1.0 spg water. The water content in the Kaolite corresponds to the dry condition (VF= 0.0287) where neutronic interaction between the packages of an array is maximized.

An infinite array of packages is evaluated in order to eliminate any biases arising from spectral leakage effects in the reflector of the finite array. The k_{eff} values for each KENO V.a case are based on 500,000 neutron histories produced by running for 215 generations with 2,500 neutrons per generation and truncating the first 15 generations of data. Each package modeled has 36 kg of 100% enriched uranium in the form of broken metal content.

Each case is rerun using a different starting random number in order to produce sets of computed k_{eff} values that are statistically independent. The random starting number, the mean value (k_{eff}), and the corresponding standard error (s_i) computed for ten individual runs are shown in Tables 6.9.2.2-1, -2, and -3. The same statistical method (described in DAC-FS-900000-A014) used in the evaluation of Kaolite models (Appendix 6.9.3, Sect. 6.9.3.4) is also used here for determining whether or not differences in neutronic performance between the package models are statistically significant.

Table 6.9.2.1-1. Deformation of the ES-3100 drum at five node points, projected by finite element analysis "Case 3100 RUN1HL Lower Bound Kaolite May 2004"

Deformation point	FEA node	Diameter at 90° (in.)	Diameter at 180° (in.)	Equivalent circular diameter	
				(in.)	(cm)
UR	098194	20.02	15.60	17.6724	44.8878
MUR	100238	20.74	15.07	17.6791	44.9050
MR	101589	20.74	14.18	17.1492	43.5588
MLR	103012	22.00	13.44	17.1954	43.6762
LR	105786	20.92	12.92	16.4404	41.7586

Table 6.9.2.1-2. Parameter changes for converting an NCT package model into an HAC package model

Parameter	Reference NCT package model	HAC model at MR node point of package	HAC model at MLR node point of package	HAC model at LR node point of package
Package Model Dimension				
OR_{Drum} (cm)	23.32990	21.77942	21.83809	20.87929
IR_{Drum} (cm)	23.17750	21.62702	21.68569	20.72689
$th_{Drum\ wall}$ (cm)	0.15240	0.15240	0.15240	0.15240
OR_{Lid} (cm)	23.11400	21.56352	21.62219	20.66339
IR_{Lid} (cm)	22.96160	21.41112	21.46979	20.51099
$th_{Kaolite}$ (cm)	12.10310	10.55262	10.61129	9.65249
Kaolite of the Body Weldment Inner Liner				
Mass (g)	117563.0	97080.4	97829.7	85839.8
Volume (cm^3)	134888.0	111387.0	112246.0	98489.5
Volume fraction multiplier [a]	–	1.21099	1.20171	1.36956
VF for water component of Kaolite	0.52294	0.63327 [b]	0.62843 [b]	0.71620 [b]
VF for dry mix component of Kaolite	0.34864	0.42220 [b]	0.41897 [b]	0.47749 [b]
Angle Iron				
Mass (g)	5621.76	4521.40	4561.66	3917.54
Volume (cm^3)	708.030	569.446	574.516	493.393
VF	1.0	1.24337	1.23239	1.43502
Drum Steel				
Mass (g)	25446.3	23397.6	23474.2	22231.2
Volume (cm^3)	3204.82	2946.80	2956.50	2799.90
VF	1.0	1.08756	1.08401	1.14462

[a] Volume fraction multiplier is an NCT density multiplier for conserving mass in components having modified volumes in the HAC calculation models.

[b] Volume Fraction (VF) for Kaolite components calculated by multiplying the VF used in the NCT model by volume fraction multiplier for the HAC model.

Table 6.9.2.2-1. Neutron multiplication factors with standard deviations for the ES-3100 package models at the "MR" and "MLR" node points

moifr	Random Number	"A" cases	k_{eff}	s	"B" cases	k_{eff}	s
1.0e-20	109E77866CF6	mrandnum_01_01	1.04965	0.00119	lrrandnum_01_01	1.05093	0.00133
1.0e-20	16AA4A58735C	mrandnum_01_02	1.05132	0.00131	lrrandnum_01_02	1.05009	0.00118
1.0e-20	1814171B652A	mrandnum_01_03	1.05368	0.00123	lrrandnum_01_03	1.05057	0.00118
1.0e-20	1A423B9472C7	mrandnum_01_04	1.05165	0.00145	lrrandnum_01_04	1.05066	0.00120
1.0e-20	20E876D82248	mrandnum_01_05	1.05344	0.00106	lrrandnum_01_05	1.04882	0.00129
1.0e-20	3F6E65CA7440	mrandnum_01_06	1.05188	0.00157	lrrandnum_01_06	1.05316	0.00127
1.0e-20	479D21DB7509	mrandnum_01_07	1.05149	0.00148	lrrandnum_01_07	1.05229	0.00134
1.0e-20	55D4371D3A23	mrandnum_01_08	1.05083	0.00113	lrrandnum_01_08	1.05186	0.00131
1.0e-20	6E1A14672B8F	mrandnum_01_09	1.04910	0.00106	lrrandnum_01_09	1.05236	0.00113
1.0e-20	77A0308C0E44	mrandnum_01_10	1.05254	0.00106	lrrandnum_01_10	1.05098	0.00120
1.0e-04	109E77866CF6	mrandnum_03_01	1.04994	0.00132	lrrandnum_03_01	1.05122	0.00123
1.0e-04	16AA4A58735C	mrandnum_03_02	1.05023	0.00118	lrrandnum_03_02	1.05324	0.00121
1.0e-04	1814171B652A	mrandnum_03_03	1.05090	0.00139	lrrandnum_03_03	1.05143	0.00123
1.0e-04	1A423B9472C7	mrandnum_03_04	1.05072	0.00115	lrrandnum_03_04	1.05048	0.00121
1.0e-04	20E876D82248	mrandnum_03_05	1.05052	0.00119	lrrandnum_03_05	1.05095	0.00137
1.0e-04	3F6E65CA7440	mrandnum_03_06	1.05383	0.00131	lrrandnum_03_06	1.05029	0.00119
1.0e-04	479D21DB7509	mrandnum_03_07	1.05205	0.00153	lrrandnum_03_07	1.05124	0.00108
1.0e-04	55D4371D3A23	mrandnum_03_08	1.05343	0.00106	lrrandnum_03_08	1.05080	0.00116
1.0e-04	6E1A14672B8F	mrandnum_03_09	1.04831	0.00132	lrrandnum_03_09	1.05074	0.00122
1.0e-04	77A0308C0E44	mrandnum_03_10	1.05353	0.00111	lrrandnum_03_10	1.05094	0.00111
0.10	109E77866CF6	mrandnum_06_01	0.97948	0.00120	lrrandnum_06_01	0.98315	0.00118
0.10	16AA4A58735C	mrandnum_06_02	0.98104	0.00125	lrrandnum_06_02	0.98605	0.00124
0.10	1814171B652A	mrandnum_06_03	0.98056	0.00134	lrrandnum_06_03	0.98690	0.00120
0.10	1A423B9472C7	mrandnum_06_04	0.97895	0.00114	lrrandnum_06_04	0.98347	0.00126
0.10	20E876D82248	mrandnum_06_05	0.98058	0.00113	lrrandnum_06_05	0.98770	0.00124
0.10	3F6E65CA7440	mrandnum_06_06	0.97966	0.00119	lrrandnum_06_06	0.98734	0.00140
0.10	479D21DB7509	mrandnum_06_07	0.97953	0.00145	lrrandnum_06_07	0.98417	0.00133
0.10	55D4371D3A23	mrandnum_06_08	0.97993	0.00130	lrrandnum_06_08	0.98712	0.00136
0.10	6E1A14672B8F	mrandnum_06_09	0.97972	0.00138	lrrandnum_06_09	0.98533	0.00142
0.10	77A0308C0E44	mrandnum_06_10	0.98157	0.00134	lrrandnum_06_10	0.98412	0.00116
0.30	109E77866CF6	mrandnum_08_01	0.93412	0.00118	lrrandnum_08_01	0.93910	0.00146
0.30	16AA4A58735C	mrandnum_08_02	0.93227	0.00138	lrrandnum_08_02	0.93757	0.00117
0.30	1814171B652A	mrandnum_08_03	0.93390	0.00131	lrrandnum_08_03	0.93940	0.00146
0.30	1A423B9472C7	mrandnum_08_04	0.93252	0.00144	lrrandnum_08_04	0.93676	0.00130
0.30	20E876D82248	mrandnum_08_05	0.93334	0.00132	lrrandnum_08_05	0.93851	0.00111
0.30	3F6E65CA7440	mrandnum_08_06	0.93168	0.00132	lrrandnum_08_06	0.93914	0.00149
0.30	479D21DB7509	mrandnum_08_07	0.93514	0.00123	lrrandnum_08_07	0.94011	0.00131
0.30	55D4371D3A23	mrandnum_08_08	0.93564	0.00132	lrrandnum_08_08	0.93900	0.00139
0.30	6E1A14672B8F	mrandnum_08_09	0.93597	0.00136	lrrandnum_08_09	0.93781	0.00117
0.30	77A0308C0E44	mrandnum_08_10	0.93525	0.00128	lrrandnum_08_10	0.93965	0.00118

Table 6.9.2.2-1. Neutron multiplication factors with standard deviations for the ES-3100 package models at the "MR" and "MLR" node points

moifr	Random Number	"A" cases	k_{eff}	s	"B" cases	k_{eff}	s
1.00	109E77866CF6	mrandnum_15_01	0.93103	0.00139	lrrandnum_15_01	0.93344	0.00126
1.00	16AA4A58735C	mrandnum_15_02	0.93082	0.00131	lrrandnum_15_02	0.93281	0.00121
1.00	1814171B652A	mrandnum_15_03	0.92890	0.00148	lrrandnum_15_03	0.93468	0.00132
1.00	1A423B9472C7	mrandnum_15_04	0.93062	0.00145	lrrandnum_15_04	0.93592	0.00126
1.00	20E876D82248	mrandnum_15_05	0.93055	0.00125	lrrandnum_15_05	0.93251	0.00143
1.00	3F6E65CA7440	mrandnum_15_06	0.92950	0.00117	lrrandnum_15_06	0.93374	0.00121
1.00	479D21DB7509	mrandnum_15_07	0.92952	0.00116	lrrandnum_15_07	0.93572	0.00138
1.00	55D4371D3A23	mrandnum_15_08	0.92805	0.00154	lrrandnum_15_08	0.93498	0.00145
1.00	6E1A14672B8F	mrandnum_15_09	0.93117	0.00140	lrrandnum_15_09	0.93224	0.00114
1.00	77A0308C0E44	mrandnum_15_10	0.93218	0.00120	lrrandnum_15_10	0.93158	0.00131

Table 6.9.2.2-2.Neutron multiplication factors with standard deviations for the ES-3100 package models at the "MLR" and "LR" node points

moifr	Random Number	"A" cases	k_{eff}	s	"B" cases	k_{eff}	s
1.0e-20	109E77866CF6	mlrrandnum_01_01	1.05024	0.00139	lrrandnum_01_01	1.05093	0.00133
1.0e-20	16AA4A58735C	mlrrandnum_01_02	1.05051	0.00135	lrrandnum_01_02	1.05009	0.00118
1.0e-20	1814171B652A	mlrrandnum_01_03	1.05121	0.00128	lrrandnum_01_03	1.05057	0.00118
1.0e-20	1A423B9472C7	mlrrandnum_01_04	1.04954	0.00120	lrrandnum_01_04	1.05066	0.00120
1.0e-20	20E876D82248	mlrrandnum_01_05	1.05249	0.00110	lrrandnum_01_05	1.04882	0.00129
1.0e-20	3F6E65CA7440	mlrrandnum_01_06	1.04924	0.00132	lrrandnum_01_06	1.05316	0.00127
1.0e-20	479D21DB7509	mlrrandnum_01_07	1.05105	0.00111	lrrandnum_01_07	1.05229	0.00134
1.0e-20	55D4371D3A23	mlrrandnum_01_08	1.05039	0.00129	lrrandnum_01_08	1.05186	0.00131
1.0e-20	6E1A14672B8F	mlrrandnum_01_09	1.05161	0.00125	lrrandnum_01_09	1.05236	0.00113
1.0e-20	77A0308C0E44	mlrrandnum_01_10	1.05041	0.00129	lrrandnum_01_10	1.05098	0.00120
1.0e-04	109E77866CF6	mlrrandnum_03_01	1.05108	0.00151	lrrandnum_03_01	1.05122	0.00123
1.0e-04	16AA4A58735C	mlrrandnum_03_02	1.05245	0.00116	lrrandnum_03_02	1.05324	0.00121
1.0e-04	1814171B652A	mlrrandnum_03_03	1.05169	0.00138	lrrandnum_03_03	1.05143	0.00123
1.0e-04	1A423B9472C7	mlrrandnum_03_04	1.05303	0.00102	lrrandnum_03_04	1.05048	0.00121
1.0e-04	20E876D82248	mlrrandnum_03_05	1.05191	0.00115	lrrandnum_03_05	1.05095	0.00137
1.0e-04	3F6E65CA7440	mlrrandnum_03_06	1.05017	0.00110	lrrandnum_03_06	1.05029	0.00119
1.0e-04	479D21DB7509	mlrrandnum_03_07	1.05232	0.00128	lrrandnum_03_07	1.05124	0.00108
1.0e-04	55D4371D3A23	mlrrandnum_03_08	1.05100	0.00144	lrrandnum_03_08	1.05080	0.00116
1.0e-04	6E1A14672B8F	mlrrandnum_03_09	1.05046	0.00145	lrrandnum_03_09	1.05074	0.00122
1.0e-04	77A0308C0E44	mlrrandnum_03_10	1.05130	0.00134	lrrandnum_03_10	1.05094	0.00111

Table 6.9.2.2-2.Neutron multiplication factors with standard deviations for the ES-3100 package models at the "MLR" and "LR" node points

moifr	Random Number	"A" cases	k_{eff}	s	"B" cases	k_{eff}	s
0.1	109E77866CF6	mlrrandnum_06_01	0.98071	0.00129	lrrandnum_06_01	0.98315	0.00118
0.1	16AA4A58735C	mlrrandnum_06_02	0.98006	0.00110	lrrandnum_06_02	0.98605	0.00124
0.1	1814171B652A	mlrrandnum_06_03	0.98043	0.00116	lrrandnum_06_03	0.98690	0.00120
0.1	1A423B9472C7	mlrrandnum_06_04	0.98253	0.00109	lrrandnum_06_04	0.98347	0.00126
0.1	20E876D82248	mlrrandnum_06_05	0.98256	0.00135	lrrandnum_06_05	0.98770	0.00124
0.1	3F6E65CA7440	mlrrandnum_06_06	0.98093	0.00127	lrrandnum_06_06	0.98734	0.00140
0.1	479D21DB7509	mlrrandnum_06_07	0.97959	0.00127	lrrandnum_06_07	0.98417	0.00133
0.1	55D4371D3A23	mlrrandnum_06_08	0.98033	0.00111	lrrandnum_06_08	0.98712	0.00136
0.1	6E1A14672B8F	mlrrandnum_06_09	0.97940	0.00117	lrrandnum_06_09	0.98533	0.00142
0.1	77A0308C0E44	mlrrandnum_06_10	0.98318	0.00134	lrrandnum_06_10	0.98412	0.00116
0.3	109E77866CF6	mlrrandnum_08_01	0.93254	0.00147	lrrandnum_08_01	0.93910	0.00146
0.3	16AA4A58735C	mlrrandnum_08_02	0.93186	0.00142	lrrandnum_08_02	0.93757	0.00117
0.3	1814171B652A	mlrrandnum_08_03	0.93200	0.00135	lrrandnum_08_03	0.93940	0.00146
0.3	1A423B9472C7	mlrrandnum_08_04	0.93197	0.00150	lrrandnum_08_04	0.93676	0.00130
0.3	20E876D82248	mlrrandnum_08_05	0.93601	0.00124	lrrandnum_08_05	0.93851	0.00111
0.3	3F6E65CA7440	mlrrandnum_08_06	0.93249	0.00118	lrrandnum_08_06	0.93914	0.00149
0.3	479D21DB7509	mlrrandnum_08_07	0.93299	0.00128	lrrandnum_08_07	0.94011	0.00131
0.3	55D4371D3A23	mlrrandnum_08_08	0.93500	0.00133	lrrandnum_08_08	0.93900	0.00139
0.3	6E1A14672B8F	mlrrandnum_08_09	0.93201	0.00122	lrrandnum_08_09	0.93781	0.00117
0.3	77A0308C0E44	mlrrandnum_08_10	0.93238	0.00153	lrrandnum_08_10	0.93965	0.00118
1.0	109E77866CF6	mlrrandnum_15_01	0.93180	0.00126	lrrandnum_15_01	0.93344	0.00126
1.0	16AA4A58735C	mlrrandnum_15_02	0.93020	0.00159	lrrandnum_15_02	0.93281	0.00121
1.0	1814171B652A	mlrrandnum_15_03	0.92956	0.00117	lrrandnum_15_03	0.93468	0.00132
1.0	1A423B9472C7	mlrrandnum_15_04	0.92837	0.00165	lrrandnum_15_04	0.93592	0.00126
1.0	20E876D82248	mlrrandnum_15_05	0.93220	0.00120	lrrandnum_15_05	0.93251	0.00143
1.0	3F6E65CA7440	mlrrandnum_15_06	0.93177	0.00141	lrrandnum_15_06	0.93374	0.00121
1.0	479D21DB7509	mlrrandnum_15_07	0.93217	0.00144	lrrandnum_15_07	0.93572	0.00138
1.0	55D4371D3A23	mlrrandnum_15_08	0.92921	0.00125	lrrandnum_15_08	0.93498	0.00145
1.0	6E1A14672B8F	mlrrandnum_15_09	0.92980	0.00177	lrrandnum_15_09	0.93224	0.00114
1.0	77A0308C0E44	mlrrandnum_15_10	0.93070	0.00126	lrrandnum_15_10	0.93158	0.00131

Table 6.9.2.2-3.Neutron multiplication factors with standard deviations for the ES-3100 package models at the "MR" and "LR" node points

moifr	Random Number	"A" cases	k_{eff}	s	"B" cases	k_{eff}	s
1.0e-20	109E77866CF6	mrandnum_01_01	1.04965	0.00119	lrrandnum_01_01	1.05093	0.00133
1.0e-20	16AA4A58735C	mrandnum_01_02	1.05132	0.00131	lrrandnum_01_02	1.05009	0.00118
1.0e-20	1814171B652A	mrandnum_01_03	1.05368	0.00123	lrrandnum_01_03	1.05057	0.00118
1.0e-20	1A423B9472C7	mrandnum_01_04	1.05165	0.00145	lrrandnum_01_04	1.05066	0.00120
1.0e-20	20E876D82248	mrandnum_01_05	1.05344	0.00106	lrrandnum_01_05	1.04882	0.00129
1.0e-20	3F6E65CA7440	mrandnum_01_06	1.05188	0.00157	lrrandnum_01_06	1.05316	0.00127
1.0e-20	479D21DB7509	mrandnum_01_07	1.05149	0.00148	lrrandnum_01_07	1.05229	0.00134
1.0e-20	55D4371D3A23	mrandnum_01_08	1.05083	0.00113	lrrandnum_01_08	1.05186	0.00131
1.0e-20	6E1A14672B8F	mrandnum_01_09	1.04910	0.00106	lrrandnum_01_09	1.05236	0.00113
1.0e-20	77A0308C0E44	mrandnum_01_10	1.05254	0.00106	lrrandnum_01_10	1.05098	0.00120
1.0e-04	109E77866CF6	mrandnum_03_01	1.04994	0.00132	lrrandnum_03_01	1.05122	0.00123
1.0e-04	16AA4A58735C	mrandnum_03_02	1.05023	0.00118	lrrandnum_03_02	1.05324	0.00121
1.0e-04	1814171B652A	mrandnum_03_03	1.05090	0.00139	lrrandnum_03_03	1.05143	0.00123
1.0e-04	1A423B9472C7	mrandnum_03_04	1.05072	0.00115	lrrandnum_03_04	1.05048	0.00121
1.0e-04	20E876D82248	mrandnum_03_05	1.05052	0.00119	lrrandnum_03_05	1.05095	0.00137
1.0e-04	3F6E65CA7440	mrandnum_03_06	1.05383	0.00131	lrrandnum_03_06	1.05029	0.00119
1.0e-04	479D21DB7509	mrandnum_03_07	1.05205	0.00153	lrrandnum_03_07	1.05124	0.00108
1.0e-04	55D4371D3A23	mrandnum_03_08	1.05343	0.00106	lrrandnum_03_08	1.05080	0.00116
1.0e-04	6E1A14672B8F	mrandnum_03_09	1.04831	0.00132	lrrandnum_03_09	1.05074	0.00122
1.0e-04	77A0308C0E44	mrandnum_03_10	1.05353	0.00111	lrrandnum_03_10	1.05094	0.00111
0.10	109E77866CF6	mrandnum_06_01	0.97948	0.00120	lrrandnum_06_01	0.98315	0.00118
0.10	16AA4A58735C	mrandnum_06_02	0.98104	0.00125	lrrandnum_06_02	0.98605	0.00124
0.10	1814171B652A	mrandnum_06_03	0.98056	0.00134	lrrandnum_06_03	0.98690	0.00120
0.10	1A423B9472C7	mrandnum_06_04	0.97895	0.00114	lrrandnum_06_04	0.98347	0.00126
0.10	20E876D82248	mrandnum_06_05	0.98058	0.00113	lrrandnum_06_05	0.98770	0.00124
0.10	3F6E65CA7440	mrandnum_06_06	0.97966	0.00119	lrrandnum_06_06	0.98734	0.00140
0.10	479D21DB7509	mrandnum_06_07	0.97953	0.00145	lrrandnum_06_07	0.98417	0.00133
0.10	55D4371D3A23	mrandnum_06_08	0.97993	0.00130	lrrandnum_06_08	0.98712	0.00136
0.10	6E1A14672B8F	mrandnum_06_09	0.97972	0.00138	lrrandnum_06_09	0.98533	0.00142
0.10	77A0308C0E44	mrandnum_06_10	0.98157	0.00134	lrrandnum_06_10	0.98412	0.00116
0.30	109E77866CF6	mrandnum_08_01	0.93412	0.00118	lrrandnum_08_01	0.93910	0.00146
0.30	16AA4A58735C	mrandnum_08_02	0.93227	0.00138	lrrandnum_08_02	0.93757	0.00117
0.30	1814171B652A	mrandnum_08_03	0.93390	0.00131	lrrandnum_08_03	0.93940	0.00146
0.30	1A423B9472C7	mrandnum_08_04	0.93252	0.00144	lrrandnum_08_04	0.93676	0.00130
0.30	20E876D82248	mrandnum_08_05	0.93334	0.00132	lrrandnum_08_05	0.93851	0.00111
0.30	3F6E65CA7440	mrandnum_08_06	0.93168	0.00132	lrrandnum_08_06	0.93914	0.00149
0.30	479D21DB7509	mrandnum_08_07	0.93514	0.00123	lrrandnum_08_07	0.94011	0.00131
0.30	55D4371D3A23	mrandnum_08_08	0.93564	0.00132	lrrandnum_08_08	0.93900	0.00139
0.30	6E1A14672B8F	mrandnum_08_09	0.93597	0.00136	lrrandnum_08_09	0.93781	0.00117
0.30	77A0308C0E44	mrandnum_08_10	0.93525	0.00128	lrrandnum_08_10	0.93965	0.00118

Table 6.9.2.2-3.Neutron multiplication factors with standard deviations for the ES-3100 package models at the "MR" and "LR" node points

moifr	Random Number	"A" cases	k_{eff}	s	"B" cases	k_{eff}	s
1.00	109E77866CF6	mrandnum_15_01	0.93103	0.00139	lrrandnum_15_01	0.93344	0.00126
1.00	16AA4A58735C	mrandnum_15_02	0.93082	0.00131	lrrandnum_15_02	0.93281	0.00121
1.00	1814171B652A	mrandnum_15_03	0.92890	0.00148	lrrandnum_15_03	0.93468	0.00132
1.00	1A423B9472C7	mrandnum_15_04	0.93062	0.00145	lrrandnum_15_04	0.93592	0.00126
1.00	20E876D82248	mrandnum_15_05	0.93055	0.00125	lrrandnum_15_05	0.93251	0.00143
1.00	3F6E65CA7440	mrandnum_15_06	0.92950	0.00117	lrrandnum_15_06	0.93374	0.00121
1.00	479D21DB7509	mrandnum_15_07	0.92952	0.00116	lrrandnum_15_07	0.93572	0.00138
1.00	55D4371D3A23	mrandnum_15_08	0.92805	0.00154	lrrandnum_15_08	0.93498	0.00145
1.00	6E1A14672B8F	mrandnum_15_09	0.93117	0.00140	lrrandnum_15_09	0.93224	0.00114
1.00	77A0308C0E44	mrandnum_15_10	0.93218	0.00120	lrrandnum_15_10	0.93158	0.00131

6.9.2.3 STATISTICAL EVALUATION

An evaluation of KENO V.a calculation results is made to determine if there is a statistically significant difference between the mean k_{eff} for the "MR" and "MLR" models, for the "MLR" and "LR" models, and for the "MR" and "LR" models. Cases are classified into five groups based on the amount of water assumed to be present in the shipping package. The symbol "I" is used to specify the case. The mean difference and standard deviation for each of the five sets of pair-wise differences are defined as follows:

(a) $d_i = (k_{effBi} - k_{effAi})/n$ and
(b) $s_{di} = \sqrt{[\, n\Sigma d_i^{\,2} - (\Sigma d_i)^2 \,] / n(n-1)}$ (conservatively defined for the t-test appropriate for small sample sizes),

where A_i and B_i denote the model types, and n denotes the sample size of ten. It is reasonable to assume that the paired differences have been randomly selected from a normally distributed population of paired differences with mean (μ_d) and standard deviation (σ_d), then the sampling distribution of

$$(d - \mu_d) / (s_d/\sqrt{n})$$

is a *t* distribution having n-1 degrees of freedom.

The evaluation of the mean differences (d_i) for the 10 sets of cases is accomplished through hypothesis testing, a statistical tool used to provide evidence that a difference exists or does not exist. The t_i values are given in Table 6.9.2.3-1. A value of 3.25 is obtained from the standard table for critical values for the t distribution from which the decision to accept or reject the null hypothesis H_0 is made with a Type I error probability (α) of 0.01.

For $|t| < 3.25$, the H_o hypothesis is not rejected. Acceptance of the null hypothesis is the result of insufficient evidence to reject it. Thus, it can be concluded that the mean estimates of the difference in k_{eff} between the "MR" and "MLR" calculation models, between the "MLR" and "LR" calculation models, and between the "MR" and "LR" calculation models are not statistically significant for the dry condition where neutronic interaction between packages is significant. Also, the mean estimate of the difference in k_{eff} between the "MR" and "MLR" calculation models is not statistically significant for wet or flooded conditions where the packages of the array become isolated.

Table 6.9.2.3-1. T-test values for establishing the statistical significance of the differences in calculated k_{eff} values for the ES-3100 package models at the "MR," "MLR," and "LR" node points

moifr	"MR" cases (k_{eff})	"MLR" cases (k_{eff})	d_i	S_{di}	t[a]
1.0E-20	1.05154	1.05075	0.00089	1.58991e-03	1.77
1.0E-04	1.05146	1.05165	-0.00019	2.17840e-03	-0.28
0.1	0.98008	0.98091	-0.00087	1.33870e-03	-2.06
0.3	0.93404	0.93300	0.00106	1.88912e-03	1.77
1.0	0.93030	0.93067	-0.00034	1.68664e-03	-0.65
moifr	**"MLR" cases (k_{eff})**	**"LR" cases (k_{eff})**	**d_i**	**S_{di}**	**t**
1.0E-20	1.05075	1.05116	-0.00050	1.92087e-03	-0.83
1.0E-04	1.05165	1.05113	0.00041	9.36819e-04	1.38
0.1	0.98091	0.98546	-0.00456	2.28535e-03	-6.31
0.3	0.93300	0.93863	-0.00578	1.59574e-03	-11.45
1.0	0.93067	0.93369	-0.00318	2.30797e-03	-4.36
moifr	**"MR" cases (k_{eff})**	**"LR" cases (k_{eff})**	**d_i**	**S_{di}**	**t**
1.0E-20	1.05154	1.05116	0.00039	2.35840e-03	0.52
1.0E-04	1.05146	1.05113	0.00021	2.19813e-03	0.31
0.10	0.98008	0.98546	-0.00543	1.66324e-03	-10.33
0.30	0.93404	0.93863	-0.00472	1.46294e-03	-10.21
1.00	0.93030	0.93369	-0.00353	2.50750e-03	-4.45

[a] critical value = 3.25 for 10 cases.

For $|t| > 3.25$, the H_o hypothesis is rejected. Therefore, it can be concluded that the mean estimate of the difference in k_{eff} between the "MLR" and "LR" calculation models, and between the "MR" and "LR" calculation models, is statistically significant for wet or flooded conditions where the packages of the array become isolated. The negative t-values indicate that the calculated k_{eff} value for the "LR" model is slightly higher than for the "MR" and "MLR" models. This result is consistent with an expected increase in k_{eff} due to "tighter or closer" water reflector surrounding the package content.

Although flattening of the side of the package represents a reduction in the diameter of the drum, the points at which minimum flattening occurs provide an indication of the reduction of lattice spacing between packages of an array under HAC. The composite of the minimum deformation points at perpendicular axes (90–270° and 0–180°) represents the modified lattice spacing in an array of ES-3100 packages. As illustrated in Table 6.9.2.3-2, the equivalent diameter of the package for "composite" lattice spacing is not significantly different from the 18.37-in. diameter of the pre-test package. Even though significant crushing of the drum midsection and bottom occurs, the effective center-to-center spacing of the contents actually increases under HAC. Selective rearrangement of alternating packages would be required to achieve a more compact array; however, this event is not credible.

As described in Sect. 6.3.1.2, a close-pack (triangular-pitch) array of packages would be represented by a reduced package in a rectangular-pitch configuration. For HAC, the 17.26-in. reduced diameter for the "composite close-pack" package is slightly larger than the 17.20-in. diameter of the "MLR" calculation model used in the HAC calculations of Sect. 6.6. Therefore, packages evaluated with the "MLR" calculation model of packages in a rectangular-pitch configuration are deemed adequate for the HAC criticality evaluation. Considering both the irregular shape of the deformed drums and that array spacing is determined by overall (maximum) dimensions rather than by mean or minimum dimensions of a damaged package, the use of the "MLR" model for representing the ES-3100 package under HAC is conservative and bounding.

Table 6.9.2.3-2. Deformation of the ES-3100 drum projected by finite element analysis "Case 3100 RUN1HL Lower Bound Kaolite May 2004"

	FEA node	Diameter at 90° (in.)	Diameter at 180° (in.)	Equivalent circular diameter (in.)
Composite	103012/098194	22.00	15.60	18.56
Pre-test drum	-	18.37	18.37	
Pre-test, close-pack	-	17.08	17.08	
Composite, close-pack	103012/098194	-	-	17.26

Appendix 6.9.3

PACKAGE MATERIAL COMPOSITIONS

Appendix 6.9.3

PACKAGE MATERIAL COMPOSITIONS

Table 6.4 (Sect. 6.3.2) provides basic information for deriving the compositions for the ES-3100 package (Figs. 6.1 and 6.2). The atomic densities presented in Table 6.4 can be verified using additional information provided in Appendix 6.9.5. The following sections provide the rationale, the justification, or both for the material compositions used in the criticality calculations.

6.9.3.1 HEU, UNIRRADIATED TRIGA AND RESEARCH REACTOR RELATED CONTENTS

HEU considered for shipment in the ES-3100 is categorized into the following material forms: highly enriched uranium (HEU) solid or broken metal; HEU oxide; uranyl nitrate hexahydrate (UNH) crystals. In the interest of adding conservatism, uranium is modeled as ^{235}U and ^{238}U, while the ^{234}U and ^{236}U isotopes are excluded. Any positive change in neutron multiplication represented by the presence of the ^{234}U is covered by the higher than actual ^{235}U content. (Rothe et al. 1978) The theoretical density of 100 wt % ^{235}U HEU is 18.8111 g/cm^3. This value is determined by adjusting the density of natural uranium included in the SCALE Standard Composition Library with 100 wt % weight factors. The theoretical density of HEU oxide types are 10.96 g/cm^3 for UO_2, 8.30 g/cm^3 for U_3O_8, and 7.29 g/cm^3 for UO_3. The theoretical density of UNH crystals is 2.79 g/cm^3. Table 6.9.3.1-1 provides details of the calculated weight percentages input to KENO V.a calculated on the basis of the stoichiometric formula of $UO_2(NO_3)_2+6H_2O$ and crystalline density. The maximum enrichment considered in the analysis is 100 wt % ^{235}U, although actual material enrichments are lower. The unirradiated solid form TRIGA fuel is uranium zirconium hydride ($UZrH_x$) where "x" is ≤2, having a density of 8.65 g/cm^3. Research reactor related contents are fuel elements or fuel components, broken metal, U-Al alloy, or oxides. These contents are described at the end of this subsection.

Table 6.9.3.1-1. Calculation of constituent weight-percentage values for uranyl nitrate hexahydrate crystals used in KENO V.a calculation models

Avogadro No. (N_o)	6.0221370E+23					
UNH $UO_2(NO_3)_2+6H_2O$	Atoms/Molecule	At. wt [a]	Mole. wt.	wt %	calc. Ni	NiAi
Hydrogen	12	1.0078	12.0936	2.4233	4.0401e+22	4.0716e+22
Nitrogen	2	14.0031	28.0062	5.6117	6.7333e+21	9.4286e+22
Oxygen	14	15.9949	223.9286	44.8690	4.7132e+22	7.5388e+23
U-235		235.0441		100.0000		
U-238		238.0510		0.0000		
Uranium	1	235.0441	235.0441	47.0962	3.3666e+21	7.9130e+23
			499.0725	100.0002		
summations				100.0002	9.7633e+22	1.6802e+24
At. Wt. material						
assumed density	2.7900					
den.=($\sum N_i A_i$)/No						2.7900

[a] *Source*: *Nuclides and Isotopes*, 14th ed., General Electric Company, 1989.

HEU broken metal. The critical mass of fissile material is dependent on factors such as the form and shape of the material, bulk density if the material is broken into pieces, and the enrichment. Broken metal can be compared to the minimum critical mass of submerged metal lattices of regular-shaped fissile material. Using experimental data, the approximation of a heterogeneous mixture of fissile material and moderator to a homogenous mixture is justified as follows.

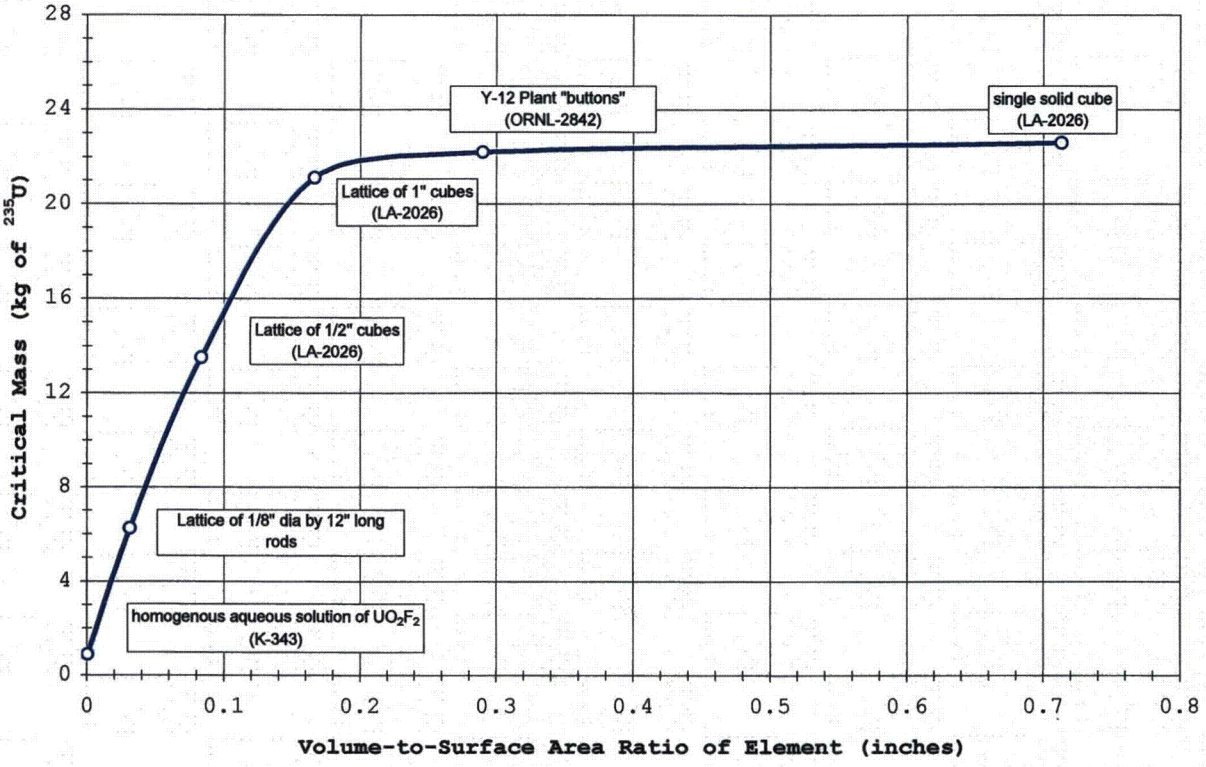

Fig. 6.9.3.1-1. Experimentally determined minimum critical mass U(~94) metal lattices immersed in water as a function of volume-to-surface area ratio of fissile material. *Source*: H. C. Paxton et al., *Critical Dimensions of Systems Containing 235U,* TID-7028, Los Alamos Scientific Lab. and Oak Ridge Natl. Lab., June 1964, Fig. 19. Y-12 data have been added.

Figure 6.9.3.1-1 depicts the experimentally determined minimum critical mass of U (~ 94) lattices immersed in water as a function of the volume-to-surface area ratio of the fissile element. (TID-7028). The critical mass is shown to increase from 850 g to 21 kg over the range of volume-to-surface ratios from 0 to 0.18 in. The critical mass is nearly constant in the range of volume-to-surface ratios from 0.18 to 0.8 in. For pieces greater than 1-in. cubes, the minimum critical mass will not be less than 21 kg. For smaller pieces, the minimum critical mass is a nearly linear function of the volume-to-surface-area ratio of the fissile element.

Figure 6.9.3.1-2 depicts the experimentally determined minimum critical mass of U (~ 94) metal water and solution systems as a function of the concentration of ^{235}U. The figure with added data reveals that: (1) a minimum critical mass exists for each metal lattice system plotted, and (2) as the bulk density of uranium or the uranium concentration increases, the curves for the critical mass of metal lattice systems converge with the curve for highly enriched solution experiments or the curve for calculated homogenous metal water mixtures. Conversely stated, the critical mass is greater for a heterogenous system than for a homogenous system, and this difference increases as the H/X ratio increases. Therefore, the practice of approximating a heterogeneous mixture of fissile material and moderator as a homogenous mixture is justifiable and also conservative at the higher H/X ratios.

Approximating broken metal as a homogenous mixture of uranium and water requires a defined space within which masses of the components are conserved. This space is generally characterized by a lattice constructed of unit cells and defined by the dimensions of the fissile material being approximated.

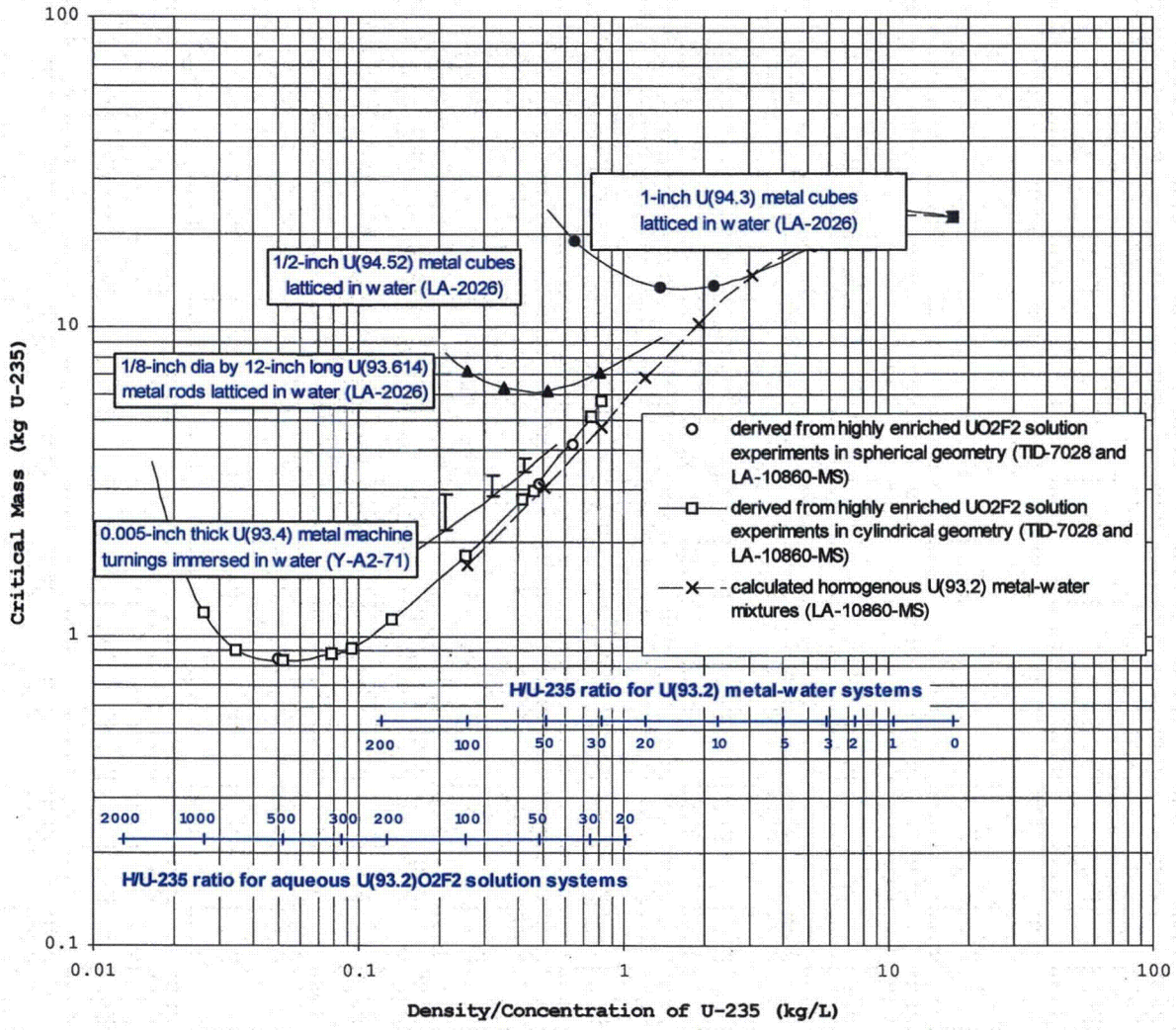

Fig. 6.9.3.1-2. Experimentally determined minimum critical mass of U(~94) metal water and solution systems as a function of the concentration of ^{235}U. *Sources*: A. W. Krass, *Survey of Experimental Data Concerning the Critical Mass of Highly Enriched Uranium–Water Systems*, CCG-365, Lockheed Martin Energy systems, Inc., Oak Ridge Y-12 Plant, July 13, 2000, Fig. 1. Y-12 data added.

The broken HEU metal consists of large, irregular pieces ranging from 0.5 in. to several inches on a side as shown in Fig. 6.9.3.1-3. A lattice of cubes is chosen to represent broken metal inside the ES-3100 containment vessel. Due to the constraints of KENO V.a, an idealized configuration is defined by a square lattice circumscribed by the inner wall of the containment vessel. Water fills the truncated cylindrical regions between the inner wall of the containment vessel and the vertical faces of the lattice. Two additional models are developed to evaluate conservatism at various stages of model approximations for broken metal.

Together, these models include an explicit arrangement of HEU metal cubes forming a compact rectangular lattice inside the containment vessel, HEU metal homogeneously mixed with water within the rectangular lattice formed by the unit cells, and HEU metal homogeneously mixed with water within the volume of the containment vessel.

Parameters varied in each of these three models include (1) the cube size in the explicit model from 1.0 in. to 0.25 in. on a side, (2) water moderation inside the containment vessel from dry to

Fig. 6.9.3.1-3. Pan of HEU broken metal.

the fully flooded condition, (3) enrichment from 100.0 wt % ^{235}U to 20.0 wt % ^{235}U, (4) thickness of the 277-4 canned spacers located between each convenience can, and (5) the mass of the uranium metal at each content location. One-quarter inch, 0.5-in., and 1.0-in. cubes are selected to evaluate "approach-to-homogeneity" of broken metal in this idealized form. The corresponding array configurations for 0.25-in., 0.5-in., and 1.0-in. cubes are 12 × 12 × N, 6 × 6 × N, and 3 × 3 × N. The N-th layer of unit cells for a given mass loading may not all contain HEU metal; the empty cells are filled with water. Nevertheless, a slight variation still arises in the total mass of HEU metal between these array configurations given whole cubes are contained in the calculation models.

The results for the calculation models representing the various configurations of broken uranium metal are shown in the Table 6.9.3.1-2. As the explicitly modeled cubes become smaller in size, the calculated k_{eff} values for the explicit "sqa" models approach values for the "lha" models where HEU metal cubes are homogenized with water within the rectangular lattice formed by the unit cells of the array. A representative or converged k_{eff} value is 0.87 for increasing by smaller cubes based on calculation results for the "lha" models. The "lha" results indicate a slight difference between the k_{eff} values for the three array sizes; these differences are attributed to the difference in the HEU for the arrays of whole cubes.

Calculation results for the "cha" models, where arrays of cubes are fully homogenized with the water for the flooded containment vessel, indicate the highest k_{eff} values. The neutron multiplication factor jumps from 0.87 to 0.95. This model is deemed to be overly conservative when applied to broken metal for the following reasons.

- HEU metal does not dissolve in water.
- HEU metal is not in an oxide or powder form that will absorb moisture or readily mix and become homogenized with the water inside the flooded containment vessel.
- Because HEU metal is much denser than water, it will not float and become distributed throughout a flooded containment vessel; instead it will gravitate toward the bottom of the containment vessel.

Table 6.9.3.1-2. Summary for evaluation of HEU broken metal models (95 wt % ^{235}U) in a flooded containment vessel, 1.4-in. canned spacers and full water reflection of containment vessel

Array type	U (g)	^{235}U (g)	H_2O (g)	h/x	k_{eff}	σ	$k_{eff} + 2\sigma$
discrete array of cubes ("sqa" cases)							
3 × 3 × *n*	35,164	33,406	7,719	6.03	0.8352	0.0012	0.84
6 × 6 × *n*	35,973	34,175	7,676	5.86	0.8559	0.0011	0.86
12 × 12 × *n*	35,988	34,188	7,765	5.86	0.8603	0.0012	0.86
cubes homogenized within footprint of lattice ("lha" cases)							
3 × 3 × *n*	35,164	33,406	7,719	6.03	0.8586	0.0011	0.86
6 × 6 × *n*	35,988	34,188	7,675	5.86	0.8650	0.0012	0.87
12 × 12 × *n*	35,988	34,188	7,675	5.86	0.8677	0.0010	0.87
cubes homogenized within containment vessel ("cha" cases)							
3 × 3 × *n*	35,164	33,406	7,719	6.03	0.9427	0.0013	0.95
6 × 6 × *n*	35,973	34,175	7,676	5.86	0.9495	0.0015	0.95
12 × 12 × *n*	35,988	34,188	7,675	5.86	0.9517	0.0016	0.95

The calculation results for the homogeneous mixture model of HEU metal and water within a rectangular lattice bound results for the explicit model. Also, the homogenization over the entire volume of the containment vessel is deemed overly conservative. For these reasons, the "lha" model is chosen to represent HEU broken metal inside the flooded containment vessel under full water reflection. For conservatism, the "cha" model is chosen to represent broken metal in single packages and the array of packages under NCT and HAC. Details about the calculation models follow.

Explicit model of HEU metal cubes forming an array of unit cells. HEU metal cubes ranging from 1.0 in. to 0.25 in. are explicitly modeled, correspondingly arranged in a 3 × 3, 6 × 6, or 12 × 12 (horizontal plane) lattice, with *N* layers vertically. The height of the lattice or the number of layers is determined by the HEU mass loading. HEU cubes are centered in the individual unit cells.

Figure 6.9.3.1-4 depicts a wire mesh view of the containment vessel and lid with three 12 × 12 × 18 arrays of HEU content separated by 277-4 canned spacers. Figure 6.9.3-1-4b depicts an isometric view of the content. The water surrounding the HEU has been removed for the purpose of the illustration. Convenience cans are not modeled; therefore, the corner unit cells nearly touch the inside wall of the containment vessel. Spacing between cubes is limited by the inner diameter of the 5.06-in. (12.8524-cm) containment vessel. The footprint of the lattice is 3.57796 in. (9.08802 cm) square. The 277-4 canned spacers are modeled as cylindrical disks with dimensions of 4.13-in. diameter × 1.37 in. height.

The HEU mass is varied in a series of calculations; however, the enrichment and density are maintained constant. The uranium mass is reduced by removing one or more cubes from the array, and the created vacancies are filled with water. Because convenience cans are not included in the calculation models, the location of the 277-4 canned spacers between the arrays decreases as complete layers of cubes are removed. The volume of the containment vessel above the top layer of the top array of cubes is filled with full-density water.

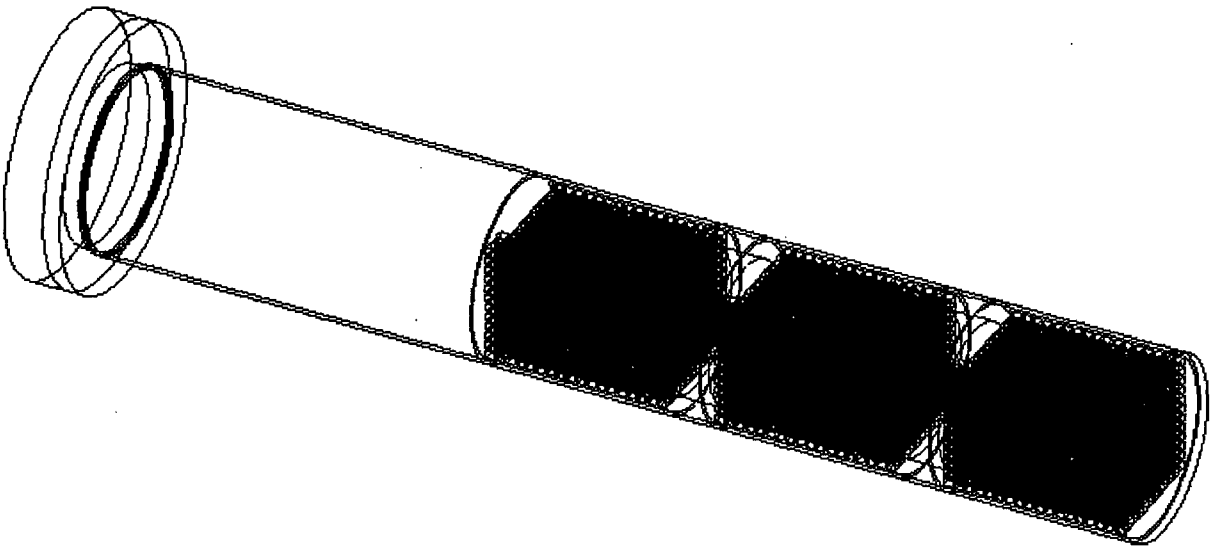

Fig. 6.9.3.1-4. Wire mesh view of the "sqa" model with three 12 × 12 × 18 lattices of HEU contents.

HEU metal homogeneously mixed with water within the rectangular lattice formed by the units cells. The HEU in the $3 \times 3 \times N$, $6 \times 6 \times N$, and $12 \times 12 \times N$ unit cells of the explicit model are homogeneously mixed with water in the rectangular lattice. Figure 6.9.3.1-5 depicts an isometric view of the homogenous "lha" model with HEU homogeneously mixed with water within the rectangular lattices formed by the unit cells. The dimensions of each rectangular lattice are defined by the 12 × 12 × 18 array of unit cells of the explicit model. Each lattice location contains the same mass of HEU and water that the respective explicit cube models contain. The volume outside the rectangular lattices is filled with full density water.

HEU metal homogeneously mixed with water within the volume of the containment vessel. The HEU in the $3 \times 3 \times N$, $6 \times 6 \times N$, and $12 \times 12 \times N$ unit cells of the explicit model are homogeneously mixed with water in the volume of the containment vessel. Figure 6.9.3.1-6 depicts an isometric cutaway view of the containment vessel and lid with HEU content homogenized with water in the containment vessel. The three rectangular lattices are used to position the 277-4 canned spacers for similarity with the "sqa" and "lha" models. The dimensions of each rectangular lattice are defined by the 12 × 12 × 18 array of unit cells of the explicit model. The mass of HEU and water of the explicit cube model is preserved.

HEU Oxide. Theoretical (crystalline) densities for HEU oxide are 10.96 g/cm^3, 8.30 g/cm^3, and 7.29 g/cm^3 for UO_2, U_3O_8, and UO_3, respectively. However, bulk densities for product oxide with enrichments ranging from 19 to 100 wt % ^{235}U are typically on the order of 6.54 g/cm^3. Therefore, only less-than-theoretical mass loadings would actually be achieved. Skull oxides are a mixture of graphite and U_3O_8 with densities on the order of 2.44 g/cm^3 for poured material and 2.78 g/cm^3 for tapped material. The combined water saturation and crystallization of the HEU oxide are not expected in the HAC, given that UO_2 and UO_3 are non-hygroscopic while U_3O_8 is only mildly hygroscopic. Table 6.9.3.1-3 provides summary data for 292 samples of canned skull oxide.

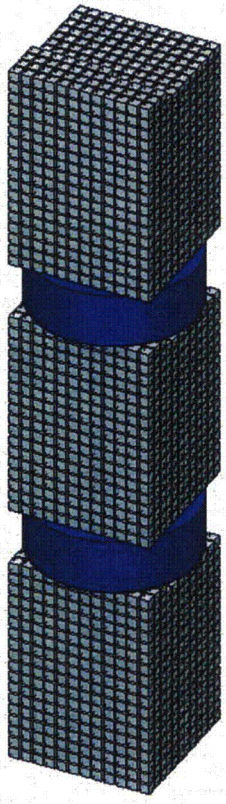

Fig. 6.9.3.1-4b. Detailed isometric view of the explicit "sqa" model for HEU broken metal. Three 12 × 12 × 18 lattices of 1-in. cubes separated by 1.4-in. 277-4 spacers are shown.

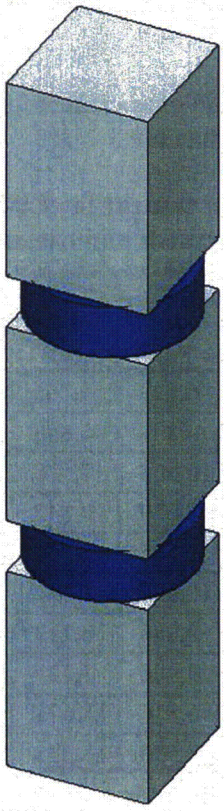

Fig. 6.9.3.1-5. Isometric view of the homogeneous "lha" model with HEU homogeneously mixed with water within the rectangular lattices formed by the units cells.

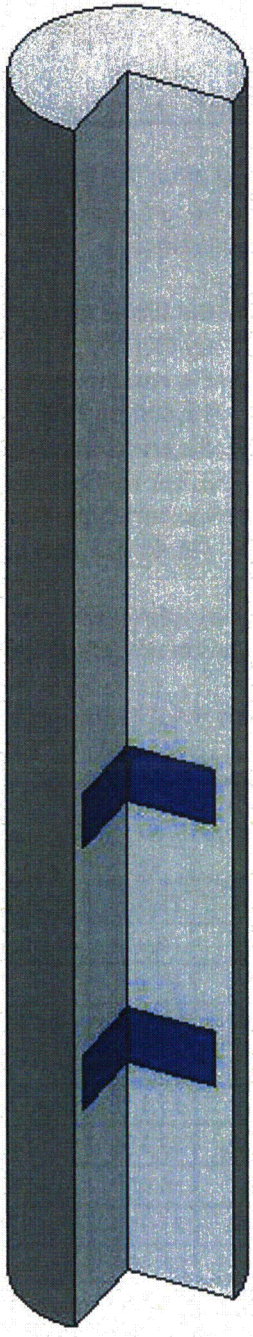

Fig. 6.9.3.1-6. Isometric view of the homogeneous "cha" model with HEU homogeneously mixed with water within the interior of the containment vessel.

Table 6.9.3.1-3. Summary data for 292 samples of skull oxide

Statistic	wt % U	wt % ^{235}U	µg C/g U	µg C /g ^{235}U	Net Wt (g)	U Wt (g)	^{235}U Wt (g)
Maximum	84.52	93.19	171,000	252,861	7,072	5,938	4,165
Minimum	12.93	20.28	13	17	442	312	221
Median	81.66	37.62	5,590	13,910	4,448	3,541	1,414
Mean	79.64	45.02	16,968	41,333	4,419	3,532	1,563
Std Dev	6.87	16.40	24,304	59,027	745	698	606

Values of wt % U, wt % ^{235}U, µg C/g U, etc. for a given statistic (maximum, minimum, medium, or mean) do not occur simultaneously in a specific sample. Inspection of sample data reveals the following characteristics:

(1) the fissile material content is ≤221 g ^{235}U in samples with concentrations up to 252,861 µg C/g^{235}U,
(2) the enrichment is 93.2 wt % ^{235}U for samples with concentrations in the range of 12,600 to 18,600 µg C/gU,
(3) the enrichment ranges from 60 to 70.2 wt % ^{235}U for samples with concentrations in the range of 3,231 to 87,720 µg C/gU, and
(4) the enrichment ranges from 37 to 38 wt % ^{235}U for samples with concentrations in the range of 400 to 233,366 µg C/gU.

Eight samples were selected and two additional ones created for establishing a bounding content calculation model. Details are provided in Table 6.9.3.1-3b.

Table 6.9.3.1-3b. Canned skull oxide (SO) content for ES-3100 calculation models, assuming 513 g polyethylene present and can spacers absent.

Content	SO (g)	UOx (g)	Sat. H_2O (g)	SO h/x	U (g)	^{235}U (g)	C (g)	µg C/ g ^{235}U	CV H_2O (g)	CV h/x	Unident (g)
sk_01	11,589	8,063	4,468	28.09	6,828	4,765	417	87,518	4,105	50.58	2,596[a]
sk_02	14,934	11,665	4,015	17.79	9,879	6,858	504	73,492	4,105	33.41	2,252[a]
sk_03	13,821	11,876	4,893	20.62	10,058	7,028	372	52,930	3,233	32.62	1,060[a]
sk_04	15,246	14,900	4,599	15.52	12,619	8,842	60	6,786	3,235	25.07	-227[b]
sk_05	21,216	21,036	3,869	9.49	17,815	12,455	27	2,168	3,235	16.27	-360[b]
sk_06	15,111	12,933	3,765	28.02	10,960	4,122	921	223,432	4,105	54.01	744[a]
sk_07	13,155	11,666	3,989	32.68	9,886	3,712	609	164,054	4,106	61.55	367[a]
sk_08	13,650	11,689	4,068	33.01	9,906	3,737	261	69,834	4,106	61.69	1,187[a]
sk_09	21,300	19,865	3,801	7.43	16,816	15,673	921	58,764	3,235	12.82	1
sk_10	21,300	20,786	3,905	7.27	17,596	16,399	0	0	3,235	12.41	1

[a] Positive value specifies grams of miscellaneous neutron absorber elements in content, modeled as water.
[b] Negative value specifies grams of excess polyethylene included in the content model.

Unirradiated TRIGA reactor fuel. TRIGA fuel is uranium zirconium hydride ($UZrH_x$), an alloy of uranium metal homogeneously dispersed as fine particles in a zirconium hydride matrix. The fuel is stable because uranium hydride does not form to any considerable extent. Moreover, uranium hydride has never been detected in the photomicrographic evaluations of TRIGA fuel.

The General Atomics catalog of stock items lists approximately 40 TRIGA fuel elements classified into four basic types: standard element, instrumented element, fuel-follower control rod, or cluster assembly. The TRIGA element active fuel region consists of three 5-in long sections "fuel meats" of $UZrH_x$. The H/Z atom ratio "x" in $UZrH_x$ equals 1.6 in all cases except for two stock items. For these cases, x = equals 1.0 and the fissile content is < 40 g ^{235}U. The unirradiated solid form TRIGA fuel is identified as either 20 % enriched or 70 % enriched, and has dimensions and material properties specific to its design function. Table 1.4 provides a summary description.

The fuel diameter for the 20 % enriched TRIGA elements is either 1.44 in., 1.41 in., 1.40 in., 1.37 in., 1.34 in., or 1.31 in. The uranium composition of the fuel is 45 wt %, 30 wt %, 20 wt %, 12 wt %, and 8.5 wt %. As illustrated in Table 6.9.3.1.4-a, the TRIGA element with a maximum fissile content of 307 g ^{235}U in 1,560 g U, 45 wt% U in $UZrH_x$, and a H/Zr atom ratio of 1.6 has a computed fuel density of ~8.66 g/cm^3. The calculated number density (N_i) for each element or isotope is also given. The TRIGA fuel element with a fuel diameter of 1.44 inches contains 3,466.7 g $UZrH_x$. Further evaluation of the manufacturers data reveals that fuel density is proportional to the uranium weight fraction. Calculated density values are: 8.6597 g/cm^3 for 45 wt% U in $UZrH_x$, 6.8995 g/cm^3 for 30 wt% U in $UZrH_x$, 6.2825 g/cm^3 for 20 wt% U in $UZrH_x$, 5.9328 g/cm^3 for 12 wt% U in $UZrH_x$, and 5.7895 g/cm^3 for 8.5 wt% U in $UZrH_x$.

The active fuel diameter for 70 % enriched TRIGA fuel is 1.44 inches in both the standard element and instrumented element, and 1.31 inches in the fuel follower control rod. The uranium composition of the fuel is 8.5 wt %. The standard element and instrumented elements contain ~136 g ^{235}U in 194 g U while the fuel follower control rod contains ~113 g ^{235}U in 162 g U. As the calculation in Table 6.9.3.1.4-b illustrates, the 70 wt % enriched TRIGA fuel has a computed density of ~5.70 g/cm^3. The TRIGA fuel element with a fuel diameter of 1.44 inches contains 2,282.4 g $UZrH_x$ while the element with a fuel diameter of 1.31 inches contains 1,888.9 g $UZrH_x$.

The clad thickness is ~0.02 inches for a TRIGA fuel element with stainless steel cladding and ~0.03 inches for an element with aluminum cladding. In preparation for shipment in the ES-3100, a TRIGA fuel element is disassembled, the fuel meats are removed from the thin cladding and packed into convenience cans.

Table 6.9.3.1-4a. Calculation of constituent weight-percentage values for 20 wt % enriched uranium-zirconium hydride content in KENO V.a calculation models

Avogadro No. (N_o) = 6.0221370e+23

$U(ZrH_x)$

atom	wt %	x	mass (g)	at. wt.		calc. N_i	N_iA_i
Hydrogen	0.9554	1.6		1.00780	1.6125	4.9439E+22	4.9824E+22
Zirconium	54.0447	1		91.21960	91.2196	3.0897E+22	2.8184E+24
u-235	19.6795		307.0	235.04410			
u-238	80.3205			238.05099			
uranium	45.0000		1560.0	237.45318	75.9535	9.8830E+21	2.3468E+24
	100.0001				168.7856		
summations	100.0001					9.0219E+22	5.2150E+24
At. wt molecule							
Volume (cm^3)	400.3200						
Mass (g)	3466.66667						
density (g/cm^3)	8.65974						
den.=(∑NiAi)/No							8.6597

Table 6.9.3.1-4b. Calculation of constituent weight-percentage values for 70 wt % enriched uranium-zirconium hydride content in KENO V.a calculation models

Avogadro No. (N_o) = 6.0221370e+23

$U(ZrH_x)$ atom	wt %	x	mass (g)	at. wt		calc. N_i	N_iA_i
Hydrogen	1.5894	1.6		1.00780	1.6125	5.4148e+22	5.4571e+22
Zirconium	89.9107	1		91.21960	91.2196	3.3841e+22	3.0870e+24
u-235	70.1031		136.0	235.04410			
u-238	29.8969			238.05099			
uranium	8.5000		194.0	235.93508	8.6237	1.2370e+21	2.9184e+23
	100.0001				101.4558		
summations	100.0001					8.9227e+22	3.4334e+24
At. wt molecule							
Volume (cm^3)	400.3200						
Mass (g)	2282.35294						
density (g/cm^3)	5.70132						
den.=(∑NiAi)/No							5.7013

The TRIGA fuel may also be configured as clad fuel rods. Each clad fuel rod will be derived from a single TRIGA fuel element by removal of the stainless steel or aluminum clad extending beyond the plenum adjacent to the axial ends of the active fuel section. Each ~15 inch long rod consists of the 3 fuel pellets and an exterior sheath of stainless steel or aluminum clad, where the protruding clad at each end has been crimped in. The fuel rods will be packed into stainless steel or tin-plated carbon steel convenience cans, with a maximum of three fuel rods per loaded convenience can. This shipping configuration requires a minimum of two convenience cans; where only one convenience can is loaded with clad fuel rods. The loaded can is 17.5 inches tall while the empty one is 8.75 inches tall. Although can spacers are not required for criticality control, can spacers or stainless steel pads may be used to take up free volume over the 31 in. internal height of the containment vessel. The maximum quantity of fissile material per package is 408 g ^{235}U.

The clad fuel rod with 1.44 inch diameter fuel pellets contains 2,282.4 g $UZrH_x$ while rod with the 1.31 inch diameter fuel pellets contains 1,888.9 g $UZrH_x$. The 0.02 in thick sheath of stainless steel clad adds ~179 g to the mass of the active fuel for the 1.48 in. diameter standard element or instrumented element, and ~163 g to active fuel mass for the 1.35 in. diameter fuel follower control rod. Allowance for 1/2 in. of residual stainless steel crimped on each end of the clad fuel rod adds ~11 - 12 g stainless steel to these amounts. Likewise, the 0.03 in thick sheath of aluminum clad adds ~90 g to the mass of the active fuel for the 1.47 in. diameter standard element or instrumented element. Allowance for 1/2 in. of residual aluminum crimped on each end of the clad fuel rod adds ~6 g aluminum.

Research reactor fuel elements or fuel components are composed of U-Al, U_3O_8-Al, or UO_2-Mg. Related materials are broken uranium metal, U-Al alloy, or oxides of U_3O_8, U_3O_8-Al, or UO_2-Mg. These items contain small quantities of fissile uranium typically ranging from 4.2 to 152 g ^{235}U. The maximum enrichment is approximately 93%. Components are of various solid shapes (rods, square bars, plates, or tubes) where diameters typically range from 0.18 to 4.0 in. and cross-sections typically range from 0.05 × 1.28 in. for an individual piece and 3.14 × 3.0 in. for an assembly of pieces. The active length for the various solid shapes ranges from 19.7 to 24 in.

U_3O_8-Al fuel elements are evaluated for demonstrating that research reactor related oxide contents are bounded by limits specified for TRIGA content. An aluminum-clad THAR plate (0.224 × 7.23 × 60.96 cm) contains approximately 101.52212 g of uranium and the enrichment is 20% ^{235}U. Table 6.9.3.1-4c presents the calculation of density values at enrichments of 20%, 70%, and 93.2% ^{235}U using plate dimensions, uranium mass, and theoretical density values of 8.3 g/cm^3 for U_3O_8 and 2.702 g/cm^3 for aluminum.

Table 6.9.3.1-4c. Calculation of constituent weight-percentage and content density values for 20 wt %, 70 wt %, and 93.2 wt % enriched uranium oxide-aluminum content in KENO V.a calculation models [a]

	Plate dimension	(cm)	Element	at. wt.	wt %	Density (g/cm^3)	Mass (g)	
	thickness	0.224	Al	26.9818	100	2.702	-	
	width	7.230	U_3O_8	variable	100	8.3	-	
	length	60.960	U	-	-	-	101.52212	
Isotope	**at. wt.**	**wt %**	**Isotope**	**at. wt.**	**wt %**	**Isotope**	**at. wt.**	**wt %**
^{235}U	235.0442	20.0	^{235}U	235.0442	70.0	^{235}U	235.0442	93.2
^{238}U	238.0510	80.0	^{238}U	238.0510	30.0	^{238}U	238.0510	6.8
U	237.4435	84.77161	U	235.9382	84.68933	U	235.2463	84.65121
O	15.9954	15.22839	O	15.9954	15.31067	O	15.9954	15.34879
U_3O_8	840.2937	100.0	U_3O_8	835.7779	100.0	U_3O_8	833.7020	100.0
Enrichment (%)	**U_3O_8 (g)**	**Vol $_{U3O8}$ (cm^3)**	**Vol $_{Al}$ (cm^3)**	**Vol $_{Total}$ (cm^3)**	**Al (g)**	**wt % $_{U3O8}$**	**wt % $_{Al}$**	**Density (g/cm^3)**
20	119.75958	14.42886	84.29707	98.72594	227.77069	34.46019	65.53981	3.52015
70	119.87593	14.44288	84.28306	98.72594	227.73282	34.48588	65.51412	3.52095
93.2	119.92992	14.44939	84.27655	98.72594	227.71524	34.49780	65.50220	3.52132

[a] Actual material at 20% enrichment, hypothetical materials at 70% and 93.2% enrichments.

A UO_2-Mg fuel element is evaluated for demonstrating that this form of research reactor related content is also bounded by limits specified for TRIGA content. An aluminum-clad EK-10 fuel rod (2.54 cm diameter and 139.7 cm length) contains approximately 92.35 g of uranium dioxide, 13.03 g of magnesium and 65.7 g of aluminum as cladding. The ^{235}U content is 8.05 g with a corresponding enrichment of 9.89%. Table 6.9.3.1-4d presents the calculation of density values at enrichments of 9.89%, 20%, and 93.2% ^{235}U using rod dimensions, material masses and theoretical density values of 10.96 g/cm^3 for UO_2 and 2.702 g/cm^3 for aluminum. For UO_2 content at 93.2% ^{235}U, an oxide density of 6.95 g/cm^3 is assumed consistent with bulk densities observed for product oxides with enrichments ranging from 19 to 100 wt % ^{235}U.

Table 6.9.3.1-4d. Calculation of constituent weight-percentage and content density values used in KENO V.a calculation models for 9.89 wt %, 20 wt %, and 93.2 wt % enriched uranium dioxide-magnesium, aluminum clad content, and for 93.2 wt % enriched uranium dioxide content [a]

		UO_2-Mg			Active	Overall	UO_2	
				Diam (cm)	0.69017	1.00000		
				Length (cm)	50.50000	55.00000		
				Vol (cm^3)	11.85982	43.19690		
		9.88 wt % ^{235}U		20 wt % ^{235}U		93.2 wt % ^{235}U	93.2 wt % ^{235}U	
	at. wt.	wt %	Mass (g)	wt %	Mass (g)	wt %	Mass (g)	wt %	Mass (g)
^{235}U	235.04420	9.88943	8.050	20.00000	16.280	93.20000	75.865	93.20000	408.000
^{238}U	238.05100	90.11057	73.350	80.00000	65.120	6.80000	5.535	6.80000	29.768
U	237.75020	88.14018	81.400	88.12668	81.400	88.02906	81.400	88.02906	437.767
O	15.99540	11.85982	10.953	11.87332	10.967	11.97094	11.069	11.97094	59.531
UO_2	269.74100		92.353		92.367		92.469		497.298
Mg	24.30480	100.00	13.030	100.00	13.030	100.00	13.030	-	-
Al	26.98180	100.00	65.670	100.00	65.670	100.00	65.67	-	-
Total			171.053		171.067		171.169		497.298
wt % U		47.58759		47.58369		47.55534		88.02906	
wt % O		6.40328		6.41096		6.46671		11.97094	
wt % Mg		7.61752		7.61690		7.61236		-	
wt % Al		38.39161		38.38846		38.36559		-	
Density (g/cm^3)		3.95984		3.96017		2.60651		6.95000	

[a] "per rod" values cited for UO_2-Mg. Actual material at 9.9% enrichment, hypothetical materials at 20% and 93.2% enrichments. Bulk values cited for UO_2.

6.9.3.2 TYPE 304 STAINLESS STEEL

The metallic components of the ES-3100 package are composed of type 304 stainless steel. These include the containment vessel, the convenience cans, the drum liner, and the drum. Type 304 stainless steel with a density of 7.9400 g/cm^3 is included as a material in the SCALE Standard Composition Library.

6.9.3.3 277-4 NEUTRON ABSORBER

Catalog No. 277 dry mix is a proprietary mixture of Thermo Electron Corporation for producing a heat-resistant shielding material which combines the most effective shielding components into a single homogeneous composite. The shielding composite material is designed to maximize the hydrogen content necessary for thermalizing fast neutrons for capture in the boron constituent. Widely used in nuclear power plant applications, the heat-resistant shielding material is capable of retaining a significant portion of its shielding properties up to 230°C (450°F). The recommended operating limit is 350°F, which is well above HAC temperatures expected inside the body weldment liner inner cavity and canned spacers.

The 277-4 neutron absorber material used in the ES-3100 is a formulation of Cat 277-0 dry mix, a boron carbide additive, and water. 277-4 is produced through a quality-controlled batch process of dry blending, wet mixing, vibration casting, and timed cure. (Equipment Specification JS-YMN3-801580-A005, Appendix 1.4.5) "Loss On Drying" (LOD) tests are used to measure the amount of water in the as-manufactured 277-4 casting. The as-manufactured 277-4 at 100 lb/ft^3 and 31.8 % LOD has a hydrogen concentration of 3.56 wt % and a natural boron concentration of 4.359 wt %. (DAC-PKG-801624-A001, Table 5)

The ability of 277-4 to perform its function depends upon the masses of hydrogen and ^{10}B locked inside the high alumina borated cement cast into the body weldment liner inner cavity and the spacer cans. A calculated amount of boron carbide is added to Cat 277-0 dry mix for producing as-manufactured 277-4 material with a volumetric isotopic concentration >7.621 × 10^{20} at/cm^3 of ^{10}B. The additive is boron carbide (B_4C) with small amount of a frit-like compound and trace amounts of unaccounted elements (0.17 wt %). Boron carbide has a theoretical density from 2.45 to 2.52 g/cm^3. The boron carbide grit partical sizes used are also small after passing through mesh sizes of 200 and 40 (63 to 355 μm). 277-4 contains a large amount of hydrated alumina, also known as aluminum trihydrate [$Al(OH)_3$]. It is a nonabrasive powder with a specific gravity of 2.42. Given that both materials are of like density and similar partial size, separation and in homogeneity of 277-4 material is not expected during the controlled vibration casting process.

Table 6.9.3.3-1 provides detailed elemental composition data derived for as-manufactured neutron absorber material at 100 lb/ft^3 and 31.8% LOD. This material description allows for clear specification of reduced boron and water contents required in the evaluation of NCT and HAC. As shown in Table 6.9.3.3-1, both the water and boron components are extracted from the material specification for the neutron absorber, and the constituent weight percents are recalculated accordingly (green box). 277-4 is specified in KENO V.a as three arbitrary materials: **arbmnpmx** with a density of 1.02276 g/cm^3, **arbmnph2o** with a density of 0.509253 g/cm^3, and **arbmboron** with a density of 6.98257e-02 g/cm^3. Model densities for 277-4 inside the body weldment liner inner cavity are reduced by a factor of 0.966893 to account for a material gap at the top of the liner. This material description allows for clear specification of reduced boron and water contents required in the evaluation of NCT and HAC.

The testing of 277-4 reveals that the material will dehydrate at elevated temperatures. Test specimens were dried at 250°F for 168 hours to reach the NCT state, and weight measurements were taken. These specimens where subsequently heated to 320°F for 4 hours to reach the HAC state, and weight measurements were again taken. The compositions of 277 at NCT and HAC states were derived by adjustment of the formulation specification for measured losses taking into account the statistical variations in the data. Conservation of mass for nonvolatile materials was observed in the derivation of material specifications based upon testing. Given that hydrogen must be present for the neutron absorber to be effective, conservative material specifications were derived for minimum hydrogen content and minimum material density.

Tables 6.9.3.3-2 and 6.9.3.3-3 respectively provide NCT and HAC composition data for as-manufactured 277-4 material at minimum density and hydrogen content. Respectively, Tables 6.9.3.3-4 and 6.9.3.3-5 provide NCT and HAC composition data or as-manufactured neutron absorber material at minimum density and boron content. Because the amount of ^{10}B present in the neutron absorber material is near saturation, a change in the hydrogen concentration has a major effect on the neutron multiplication factor, while a change in the amount of boron has a minor effect.

The neutron absorbing material used in the ES-3100 Shipping Package will perform as analyzed. The analysis of 277-4 with criticality calculations is adequate in lieu of neutron transmission testing for the demonstration of acceptable performance by experimental means. Criticality calculations show boron

content is adequate and k_{eff} is not dependent on absolute (microscopic) homogeneity. Geometry characteristics of the ES-3100 system preclude the need for uniformity in boron areal density as a prerequisite for criticality safety control. The neutron absorbing material will be fabricated under strict quality control and accepted for use under an NQA-1 compliant quality assurance (QA) program. A QA-approved mixing process provides a method for creating an exact mix for the neutron absorber during ES-3100 fabrication. An important part of this QA-approved process is a 277-4 material verification and acceptance testing program. The following discussion elaborates on these key points:

The analysis of 277-4 with criticality calculations is adequate in lieu of neutron transmission testing for the demonstration of acceptable performance. Early on in the licensing process, Borobond 4 was selected as the neutron absorber material for use in the ES-3100 package. The decision to use Borobond 4 in the ES-3100 was made because of favorable experience with its use in the Highly Enriched Uranium (HEU) Rackable Can Storage Box (RCSB), an element of the new state-of-the art HEU storage facility at the Y-12 National Security Complex (Y-12). From an economic standpoint, however, Borobond 4 proved not to be a viable option for the small quantities needed for the ES-3100 project. 277-4 neutron absorber material, which has very similar nuclear material properties to Borobond 4, was then selected as an alternative.

Both the RCSB and the ES-3100 are fast systems in the normal condition when the HEU fissile material is essentially unmoderated. A key factor for an effective neutron absorber is that hydrogen should be present for moderation, and it should be interspersed with boron-10 (^{10}B), thus promoting neutron capture. The potential for neutron streaming through an absorber is significant when a hydrogenous moderator is absent, as in the case of an aluminum boron-carbide matrix (a Boral alloy).

Borobond 4 is a ceramicrete material with slightly greater than 4 wt % boron carbide (B_4C). The boron carbide powder is micro encapsulated by the crystalline matrix of the ceramic; therefore, leaching out the boron is not feasible. In Borobond 4, 100 wt % of the B_4C has a particle size <500 μm; 90 wt % of the other constituents range from <164 μm to <36 μm. Given the differences in particle size, the potential for separation in the mixing process is real.

Some of the questions regarding the use of 277-4 as a neutron poison in the ES-3100 were previously addressed regarding the use of Borobond 4 in the RCSB. Radiography was performed on Borobond 4 samples ranging in thickness from 1.0 to 1.5 in. Inspections revealed little or no visual differences, indicating uniformity of the Borobond 4. For 277-4 where the B_4C grit is on the order of 200 μm, the potential for separation is reduced.

Measurements from neutron transmission tests on Borobond 4 for determination of areal density indicated greater boron content than was physically present. This is due to the presence of elements besides the aluminum and boron (principally hydrogen, oxygen and other low and intermediate-Z elements). From these measurements, credit for 90 wt % boron in a criticality calculation was established as an adequate adjustment. Given the similarity of 277-4 to Borobond 4 (a ceramic-cement composite shielding material, with a similar elemental composition, more uniform particle size, and the same boron content), the 75% credit for boron content applied in the ES-3100 criticality calculations is an adequate enough correction for the efficiency of the material.

Table 6.9.3.3-1. Calculation of constituent weight-percentage values used in KENO V.a calculation models for as-manufactured 277-4 at minimum acceptable density and boron content[a]

			arbmboron	arbmnpmx	arbmnph2o			arbmboron	arbmnpmx	arbmnph2o
31.8% LOD	At. wt	lb/ft^3	lb/ft^3	lb/ft^3	lb/ft^3		NID	Wt %	Wt %	Wt %
H	1.0078	3.5579			3.5579	**H**	1001			11.1913%
B10	10.0129	0.7911	0.7911			**B10**	5010	18.1482%		
B11	11.0093	3.5680	3.5680			**B11**	5011	81.8518%		
C	12.0000	1.2251		1.2251		**C**	6012		1.9187%	
N	14.0031	0.0090		0.0090		**N**	7014		0.0141%	
O	15.9949	55.9620		27.7281	28.2339	**O**	8016		43.4275%	88.8087%
Na	22.9895	0.0750		0.0750		**Na**	11023		0.1175%	
Mg	24.3051	0.2156		0.2156		**Mg**	12000		0.3377%	
Al	26.9818	24.9306		24.9306		**Al**	13027		39.0461%	
Si	28.0853	1.5752		1.5752		**Si**	14000		2.4671%	
S	32.0636	0.1969		0.1969		**S**	16000		0.3084%	
Ca	40.0803	7.5553		7.5553		**Ca**	20000		11.8331%	
Fe	55.8447	0.3383		0.3383		**Fe**	24000		0.5298%	
Totals		100.0000	4.3591	63.8491	31.7918			100.00%	100.00%	100.00%
H_2O	18.0105									
density (g/cm^3)		1.601838e+00	6.982572e-02	1.022759e+00	5.092532e-01	spacer density (g/cm^3)	1.601838e+00	6.98257e-02	1.02276e+00	5.09253e-01
						liner density (g/cm^3)	1.548806e+00	6.75140e-02	9.88899e-01	4.92393e-01
						liner den. multiplier	0.966893			

a *Source*: G. A. Byington, *Mixing Weights and Elemental Composition of 277-4 Neutron Poison Used in the ES-3100*, DAC-PKG-801624-A001, BWXT Y-12, Y-12 National Security Complex, Jan. 25, 2006, Table 5.

Table 6.9.3.3-2. Calculation of constituent weight-percentage values used in KENO V.a calculation models for NCT as-manufactured 277-4 at minimum density and hydrogen content[a]

			arbmboron	arbmnpmx	arbmnph2o			arbmboron	arbmnpmx	arbmnph2o
	At. wt	lb/ft^3	lb/ft^3	lb/ft^3	lb/ft^3		NID	Wt %	Wt %	Wt %
H	1.0078	2.6840			2.6840	**H**	1001			11.1913%
B10	10.0129	0.8282	0.8282			**B10**	5010	18.1479%		
B11	11.0093	3.7354	3.7354			**B11**	5011	81.8520%		
C	12.0000	1.2826		1.2826		**C**	6012		1.9189%	
N	14.0031	0.0094		0.0094		**N**	7014		0.0141%	
O	15.9949	50.3252		29.0262		**O**	8016		43.4251%	
O	15.9949				21.2990	**O**	8016			88.8087%
Na	22.9895	0.0785		0.0785		**Na**	11023		0.1174%	
Mg	24.3051	0.2258		0.2258		**Mg**	12000		0.3378%	
Al	26.9818	26.1004		26.1004		**Al**	13027		39.0479%	
Si	28.0853	1.6491		1.6491		**Si**	14000		2.4672%	
S	32.0636	0.2061		0.2061		**S**	16000		0.3083%	
Ca	40.0803	7.9098		7.9098		**Ca**	20000		11.8336%	
Fe	55.8447	0.3541		0.3541		**Fe**	24000		0.5298%	
Totals		95.3886	4.5636	66.8420	23.9830			100.00%	100.00%	100.00%
H_2O	18.0105									
density (g/cm^3)		1.527971e+00	7.310148e-02	1.070700e+00	3.841692e-01	spacer density (g/cm^3)	1.527971e+00	7.31015e-02	1.07070e+00	3.84169e-01
						liner density (g/cm^3)	1.477385e+00	7.06813e-02	1.03525e+00	3.71451e-01
						liner den. multiplier	0.966893			

a *Source*: G. A. Byington, *Mixing Weights and Elemental Composition of 277-4 Neutron Poison Used in the ES-3100*, DAC-PKG-801624-A001, BWXT Y-12, Y-12 National Security Complex, Jan. 25, 2006, Table 11.

Table 6.9.3.3-3. Calculation of constituent weight-percentage values used in KENO V.a calculation models for HAC as-manufactured 277-4 at minimum density and hydrogen content[a]

			arbmboron	arbmnpmx	arbmnph2o
	At. wt	lb/ft³	lb/ft³	lb/ft³	lb/ft³
H	1.0078	2.6758			2.6758
B10	10.0129	0.8282	0.8282		
B11	11.0093	3.7354	3.7354		
C	12.0000	1.2826		1.2826	
N	14.0031	0.0094		0.0094	
O	15.9949	50.2605		29.0265	
O	15.9949				21.2340
Na	22.9895	0.0785		0.0785	
Mg	24.3051	0.2258		0.2258	
Al	26.9818	26.1004		26.1004	
Si	28.0853	1.6491		1.6491	
S	32.0636	0.2061		0.2061	
Ca	40.0803	7.9098		7.9098	
Fe	55.8447	0.3541		0.3541	
Totals		95.3157	4.5636	66.8423	23.9098
H_2O	18.0105				
density (g/cm³)		1.52680e+00	7.31015e-02	1.07071e+00	3.82995e-01

		arbmboron	arbmnpmx	arbmnph2o
	NID	**Wt %**	**Wt %**	**Wt %**
H	1001			11.1913%
N10	5010	18.1479%		
N11	5011	81.8520%		
V	6012		1.9188%	
N	7014		0.0141%	
O	8016		43.4254%	
O	8016			88.8087%
Na	11023		0.1174%	
,g	12000		0.3378%	
Al	13027		39.0477%	
Si	14000		2.4671%	
S	16000		0.3083%	
Ca	20000		11.8335%	
Fe	24000		0.5298%	
		100.00%	100.00%	100.00%
spacer density (g/cm³)	1.52680e+00	7.31015e-02	1.07071e+00	3.82995e-01
liner density (g/cm³)	1.47626e+00	7.06813e-02	1.03526e+00	3.70316e-01
liner den. multiplier	0.966893			

a *Source*: G. A. Byington, *Mixing Weights and Elemental Composition of 277-4 Neutron Poison Used in the ES-3100*, DAC-PKG-801624-A001, BWXT Y-12, Y-12 National Security Complex, Jan. 25, 2006, Table 12.

Table 6.9.3.3-4. Calculation of constituent weight-percentage values used in KENO V.a calculation models for NCT as-manufactured 277-4 at minimum density and boron content[a]

			arbmboron	arbmnpmx	arbmnph2o			arbmboron	arbmnpmx	arbmnph2o
	At. wt	lb/ft^3	lb/ft^3	lb/ft^3	lb/ft^3		NID	Wt %	Wt %	Wt %
H	1.0078	2.9617			2.9617	**H**	1001			11.1913%
B10	10.0129	0.7911	0.7911			**B10**	5010	18.1482%		
B11	11.0093	3.5680	3.5680			**B11**	5011	81.8517%		
C	12.0000	1.2251		1.2251		**C**	6012		1.9188%	
N	14.0031	0.0090		0.0090		**N**	7014		0.0141%	
O	15.9949	51.2291		27.7264		**O**	8016		43.4260%	
O	15.9949				23.5027	**O**	8016			88.8087%
Na	22.9895	0.0750		0.0750		**Na**	11023		0.1175%	
Mg	24.3051	0.2156		0.2156		**Mg**	12000		0.3377%	
Al	26.9818	24.9306		24.9306		**Al**	13027		39.0472%	
Si	28.0853	1.5752		1.5752		**Si**	14000		2.4671%	
S	32.0636	0.1969		0.1969		**S**	16000		0.3084%	
Ca	40.0803	7.5553		7.5553		**Ca**	20000		11.8334%	
Fe	55.8447	0.3383		0.3383		**Fe**	24000		0.5299%	
Totals		94.6709	4.3591	63.8474	26.4644			100.00%	100.00%	100.00%
H2O	18.0105									
density (g/cm^3)		1.516474e+00	6.982572e-02	1.022731e+00	4.239172e-01	spacer density (g/cm^3)	1.516474e+00	6.98257e-02	1.02273e+00	4.23917e-01
						liner density (g/cm^3)	1.466269e+00	6.75140e-02	9.88872e-01	4.09883e-01
						liner den. multiplier	0.966893			

a *Source*: G. A. Byington, *Mixing Weights and Elemental Composition of 277-4 Neutron Poison Used in the ES-3100*, DAC-PKG-801624-A001, BWXT Y-12, Y-12 National Security Complex, Jan. 25, 2006, Table 13.

Table 6.9.3.3-5. Calculation of constituent weight-percentage values used in KENO V.a calculation models for HAC as-manufactured 277-4 at minimum density and boron content[a]

			arbmboron	arbmnpmx	arbmnph2o			arbmboron	arbmnpmx	arbmnph2o
	At. wt	lb/ft³	lb/ft³	lb/ft³	lb/ft³		NID	Wt %	Wt %	Wt %
H	1.0078	2.9524			2.9524	**H**	1001			11.1913%
B10	10.0129	0.7911	0.7911			**B10**	5010	18.1482%		
B11	11.0093	3.5680	3.5680			**B11**	5011	81.8517%		
C	12.0000	1.2251		1.2251		**C**	6012		1.9188%	
N	14.0031	0.0090		0.0090		**N**	7014		0.0141%	
O	15.9949	51.1551		27.7262		**O**	8016		43.4258%	
O	15.9949				23.4289	**O**	8016			88.8087%
Na	22.9895	0.0750		0.0750		**Na**	11023		0.1175%	
Mg	24.3051	0.2156		0.2156		**Mg**	12000		0.3377%	
Al	26.9818	24.9306		24.9306		**Al**	13027		39.0473%	
Si	28.0853	1.5752		1.5752		**Si**	14000		2.4671%	
S	32.0636	0.1969		0.1969		**S**	16000		0.3084%	
Ca	40.0803	7.5553		7.5553		**Ca**	20000		11.8334%	
Fe	55.8447	0.3383		0.3383		**Fe**	24000		0.5299%	
Totals		94.5876	4.3591	63.8472	26.3813			100.00%	100.00%	100.00%
H_2O	18.0105									
density (g/cm³)		1.515140e+00	6.982572e-02	1.022728e+00	4.225861e-01	spacer density (g/cm³)	1.515140e+00	6.98257e-02	1.02273e+00	4.22586e-01
						liner density (g/cm³)	1.464979e+00	6.75140e-02	9.88869e-01	4.08596e-01
						liner den. multiplier	0.966893			

a *Source*: G. A. Byington, *Mixing Weights and Elemental Composition of 277-4 Neutron Poison Used in the ES-3100*, DAC-PKG-801624-A001, BWXT Y-12, Y-12 National Security Complex, Jan. 25, 2006, Table 14.

Criticality calculations show boron content is adequate and k_{eff} is not dependent on absolute (microscopic) homogeneity. The boron concentration calculations presented here model an infinite array of ES-3100 packages with the boron concentration of Cat 277-4 uniformly varied inside the body weldment inner liner. While the Cat 277-4 described herein is an earlier formulation of the neutron absorber material, the behavior characteristics being demonstrated for Cat 277-4 apply to the revised formulation, 277-4.

Credit for only 75% of the boron is taken in the specification of Cat 277-4. Each package in the array contains 2.774 kg of ^{235}U in broken metal form uniformly distributed inside the containment vessel. The presence of just the hydrogenous cement matrix in the inner liner reduces k_{eff} to 1.132 from a value of 1.35 without the cement matrix. As an initial 1 wt % natural boron is added to the high alumina cement system (Table 6.9.3.3-6), the calculated k_{eff} based on 75% of the boron present drops significantly. Cat 277-4 with 4.2284 wt % natural boron in the minimum cast density of 100 lb/ft^3 (1.60 g/cc) has an acceptable mixture concentration, generating a k_{eff} of 0.88. The saturation value for boron content is reached at ~8 wt %. This near doubling of the boron content results in ~4% decrease in k_{eff} to an asymptotic value of ~0.85.

The density of Cat 277-4 is the sum of constituent densities: the boron density, the base-material density, and the water density. In the calculation model, the density of water in Cat 277-4 is 0.48210 g/cm^3 (not shown in Table 6.9.3.3-6). Canned spacers are omitted from the calculation model. Credit for only 75% of the boron is taken in each parametric calculation. The volume of the 277-4 in the body weldment inner liner cavity is 1.32708×10^4 cm^3.

Table 6.9.3.3-6. Effect of boron concentration on array neutron multiplication

100%B (wt %)	Boron density (g/cm^3)	Base material density (g/cm^3)	NP277-4 mass (g)	Case name	$k_{eff} \pm 2\sigma$ (@75% B)
0.01	0.00016	1.11775	21232.6	nbiabm_kvsb_1	1.13199 +/- 0.00138
0.1	0.0016	1.11631	2.12279E+04	nbiabm_kvsb_2	1.07944 +/- 0.00145
1	0.016	1.10191	2.11801E+04	nbiabm_kvsb_3	0.95564 +/- 0.00129
2	0.032	1.08591	2.11270E+04	nbiabm_kvsb_4	0.91708 +/- 0.00135
3	0.048	1.06991	2.10739E+04	nbiabm_kvsb_5	0.89396 +/- 0.00117
4.2284	0.068614	1.04930	2.10056E+04	nbiabm_kvsb_6	0.87985 +/- 0.00145
6	9.6000E-02	1.02191.	2.09147E+04	nbiabm_kvsb_7	0.86029 +/- 0.00151
8	1.2800E-01	0.98991	2.08085E+04	nbiabm_kvsb_8	0.84769 +/- 0.00150
10	0.16	0.95791	2.07024E+04	nbiabm_kvsb_9	0.84086 +/- 0.00142

NUREG 1609 recommended that only 75% of the minimum boron density be credited in criticality evaluation in order to address the issue of non-homogeneity of ^{10}B in the neutron absorber material. The boron non-homogenity calculations presented here model an infinite array of ES-3100 packages with the boron concentration of Cat 277-4 varying along the vertical height of the body weldment inner liner. However, the total amount of boron in each package is fixed. Each package in the array contains 2.774 kg of ^{235}U in broken metal form uniformly distributed inside the containment vessel. Two sets of calculations are evaluated with this model to address the effects of boron distribution in the ES-3100 inner liner.

In one set of cases, the inner cavity is divided vertically into three equal-volume regions. The density in one region is increased to 95% of the minimum boron density, while the boron density in the

other two regions is decreased to 65%, thus preserving the amount of neutron absorber material in the package. In the other set of cases, the inner cavity is divided vertically into four equal volume regions, but two regions are combined. This creates two quarter-sized regions and one half-size region. The density in the half-size region is increased to 95% of the minimum boron density, while the density in the quarter-sized regions is decreased to 55%, thus preserving the amount of neutron absorber in the package. In both sets of calculations, the high-density region was shifted upward in the package to examine the effect of boron distribution.

As shown in Figures 6.9.3.3-2 and 6.9.3.3-3, the effect of non-homogeneity of boron in the ES-3100 liner on k_{eff} is not statistically significant. The "65% - 95% - 65%" nonhomogeneous boron distribution represents a relative standard deviation of 23.1% in boron concentration. Given the controls on method of manufacture and installation of the neutron absorber material, these calculated conditions bound the expected physical distribution of boron with a large degree of conservatism.

Geometry characteristics of the ES-3100 system preclude the need for uniformity in boron areal density as a prerequisite for criticality safety control. The ISG-15 provides crucial guidance for controlling areal density in a geometry configuration where one-dimensional effects are significant, such as a distributed source separated by thin Boral sheets (aluminum and boron carbide) which range in thickness from 0.075 to 0.4 in. In this example, Boral aluminum sheets are placed between fissile fuel rods just a few inches away and only become efficient when the low-enriched fissile material is placed in a sea of hydrogenous moderator. The cylindrical thickness of the ES-3100 cast neutron absorber material (Cat 277-4) is 1.12 in., which is about three times thicker than the largest Boral sheet. Its purpose in the ES-3100 is to provide criticality safety control for arrays of packages.

In the ES-3100, the proposed fissile mass loads are separated by at least one drum diameter (19.36 in.). Drawing M2E801580A031 in Appendix 1.4.8 shows the cross-section view of the many different layers of materials that are between the fissile mass loads in adjacent packages in an array. The direct neutron transport path between dispersed fissile material (assuming a neutron passes through the following thickness of materials at a normal angle to the closest neighboring package) is:

- fissile material,
- 0.100 in. 304 stainless-steel containment vessel wall,
- air gap,
- 0.06 in. 304 stainless-steel inner liner wall,
- 1.12 in. of 277-4 neutron absorber material,
- 0.06 in. 304 stainless-steel outer liner wall,
- 4.77 in. of Kaolite,
- 0.06 in. 304 stainless-steel outer drum wall, and
- air gap,

followed by the reverse:

- 0.06 in. stainless-steel outer drum wall,
- 4.77 in. of Kaolite,
- 0.06 in. 304 stainless-steel outer liner wall,
- 1.12 in. of 277-4 neutron absorber material,
- 0.06 in. 304 stainless-steel inner liner wall,
- air gap,
- 0.100 in. 304 stainless-steel containment vessel wall, and
- back into a fissile material.

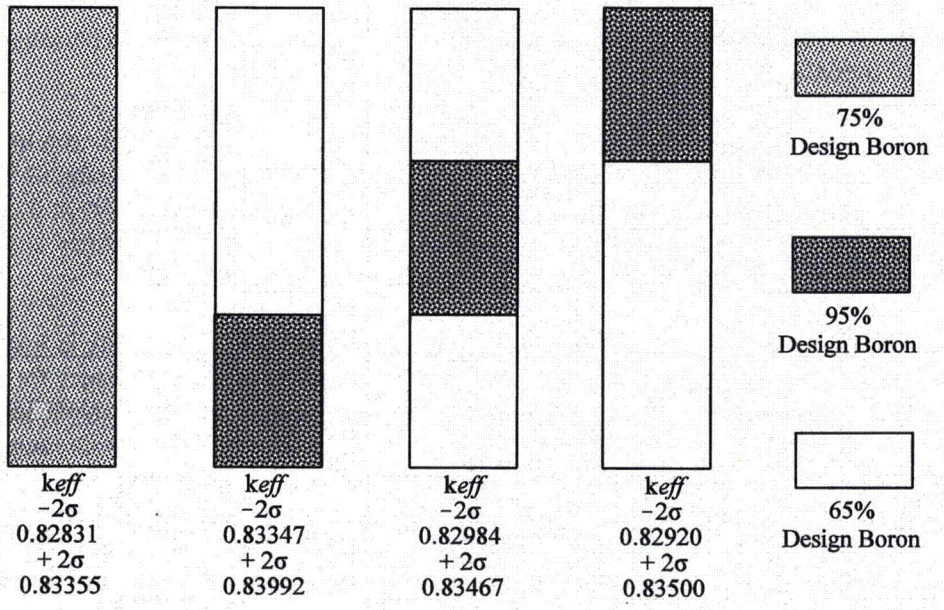

Fig. 6.9.3.3-2. Three equal-region models for evaluation of non-homogeneity in the boron distribution.

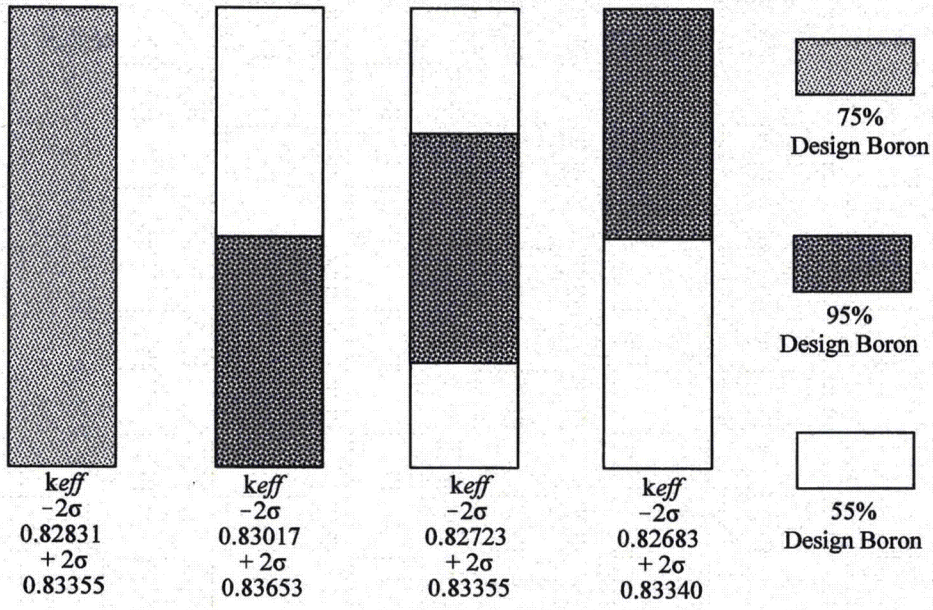

Fig. 6.9.3.3-3. Non-uniform region model for evaluation of non-homogeneity in the boron distribution.

At the shortest distance between fissile materials, neutrons travel through the 1.12 in. (2.8448 cm) of 277-4 neutron absorber material and 0.28 in. (0.7112 cm) of 304 stainless steel at least twice, with the high probability of several neutron scattering collisions along the way. Thus, the mean free path in the package is much smaller than the separation between the fissile material of adjacent packages.

In contrast to a Boral sheet application, the neutron absorber component of the ES-3100 package physically represents a significant fraction of the total container volume and is large in comparison to the potential fissile material volume. Furthermore, the neutron absorber component consists of boron dispersed throughout a hydraulic cement matrix with a high neutron scattering potential. The net result is that sensitivity to angular and spatial variations in the areal density of ^{10}B in the neutron absorber volume is eliminated.

The neutron absorbing material will be fabricated under strict quality control and accepted for use under an NQA-1 compliant QA program. The original equipment specification for the production of 277-4 neutron absorber material used a proprietary mixture from the Thermo Electron Corporation that combined high alumina cement and a boron grit (Cat 277-4). The manufacturing process for the neutron absorber was revised in order to obtain details necessary for material characterization and to achieve process control for ensuring consistency of absorber material among lots.

A two-part system of dry-blend components is now employed rather than relying on a single base material (a premixed powder of high alumina cement and boron grit). Thermo Electron Corporation's proprietary high-alumina cement without boron grit (Cat 277-0) is mixed on-site with boron carbide by the ES-3100 manufacturer under strict quality controls. A single batch is mixed on a per package basis. The boron carbide used in this process is strictly controlled. Boron carbide is specified per ASTM C 750-03, "Nuclear-Grade Boron Carbide Powder," in the Type 1 category. The grit size is controlled to ≤ 100 μm or a grit size of 120 per ANSI B74-12, with 100% passing a 120USS mesh.

The new formulation designated "277-4" is produced through a quality-controlled batch process of dry blending, wet mixing, vibration casting, and timed cure. (Equipment Specification JS-YMN3-801580-A005, Appendix 1.4.5) The plan is to control the purity, boron carbide particle size, chemistry, measurements, weights, mixing, recording, casting, and testing using one batch per each shipping package (and its two companion spacer cans). A design analysis calculation shows all of the calculations used in mixing and determines (from the minimum acceptable chemical purities) the volumetric densities in g/cm^3 and an areal density in g/cm^3 of ^{10}B. (DAC-PKG-801624-A001) These values will prove the acceptability of the mixing specifications.

An important part of this approach is a QA-approved 277-4 material verification and acceptance testing program. The applicant plans on performing 100% acceptance testing on the criticality safety significant properties of density, ^{10}B interaction (neutron absorption), and hydrogen content. The acceptance density shall be the as cast density in the drum to 105−5+10 lb/ft^3 and shall be determined as shown in Appendix 1.4.5. To test the other properties, two companion sample cans shall be cast from each batch used to cast a shipping container (the manufacturer will cast a fresh batch for each shipping container). The companion sample cans shall also have their density verified. The ^{10}B interaction will be tested in the manner described in Appendix A of the 277-4 specification (Appendix 1.4.5). Initially, a new set of 277-4–certified cans will be cast using the newly proposed casting specification with the QA plan described previously. Then, on a companion sample can for each batch pour, a Prompt Gamma-ray Neutron Activation Analysis (PGNAA) test will be used to neutronically test the ^{10}B for absorption. To pass the PGNAA test, the sample can results must be within the results obtained for the 277-4 certified standards, in units of Average Net Count rate (ANC/second) ±4 standard deviations. The second companion sample can will be used to test for hydrogen content using an LOD test as described in

Appendix 1.4.5. Upon successful completion of the density, PGNAA, and LOD testing, the ES-3100 neutron absorber material will be accepted for use.

6.9.3.4 KAOLITE 1600

Kaolite 1600, manufactured by Thermal Ceramics of Augusta, Georgia [telephone number (404) 796-4200], is a super-lightweight, low thermal conductivity, castable material designed for backup insulation up to 1600°F. The material is obtained as a dry powder with the chemical composition given in Table 6.9.3.4-1. The powder is mixed with water in a water-to-powder ratio of 14.5 qt per 20-lb bag. The mixture is poured into the drum body weldment or top plug, vibrated to eliminate voids, and then dried and fired to form the finished product. (Rowland, 2001) The density of the fired material is ~25 lb/ft^3. It is assumed that the wet mixture contains the maximum water possible. This value (14.5 qt per 20 lb) is therefore used to determine the maximum water content of the fired product,

$$S.G._{max} = \frac{14.5\ qt}{20\ lb\ dry} \times \frac{25\ lb}{ft^3} \times \frac{0.946\ \ell}{1\ qt} \times \frac{998.2\ g}{\ell} \times \frac{35.32\ ft^3}{10^6\ cm^3} = \frac{0.6045\ g}{cm^3}\ .$$

Table 6.9.3.4-1. Kaolite 1600 chemical composition, percent fired basis

Component	Weight percent	Component	Weight percent
Al_2O_3	9.6	CaO	30.7
SiO_2	36.7	MgO	13.1
Fe_2O_3	6.7	Na_2O	2.0
TiO_2	1.2		

Tables 6.9.3.4-2 and 6.9.3.4-3 provide detailed information regarding the weight measurements taken during the casting of Kaolite 1600 for the production of a series of drum body weldment and top plug parts for a similar package (the BWXT Y-12 Model ES-2100). The mean values for the amount of Kaolite and water present after baking are 107.08 lb of Kaolite and 4.8 lb of water in the drum body weldment, and 16.99 lb of Kaolite and 0.58 lb of water in the top plug. An ES-2100 package contains, on the average, 124.07 lb (56,276.91 g) of Kaolite and 5.38 lb (2,440.32 g) of water. Given that the average volume is 5.72 ft^3, the average density of Kaolite is 22.63 lb/ft^3 (0.3625 g/cm^3).

The volume of the Kaolite region in the KENO models is 1.63417 × 5 cm^3. For NCT, the density of Kaolite is 0.34438 g/cm^3, and the density of water is 0.01493 g/cm^3. The data in Tables 6.9.3.4-2 and 6.9.3.4-3 indicate that the Kaolite may have as little as 1.90 lb (861.82 g) of water after baking (Part Serial Number 97) such that the corresponding density of water is 0.00527 g/cm^3. For the water-flooded HAC, the amount of water is assumed not to exceed the amount present before baking. The package would contain on the average 186.10 lb (84,413.1 g) of water such that the corresponding density is 0.51655 g/cm^3. The full range of NCT and HAC conditions would be covered by a variation of water in the Kaolite from 0 g/cm^3 to 0.51655 g/cm^3 in a calculation model.

Table 6.9.3.4-2. Fabrication data, before and after baking the drum body weldment parts of the ES-2100 shipping package

								before baking			after baking		
Part Serial Number	clean & empty (lb)	filled with water (lb)	before baking (lb)	after baking (lb)	density after baking (lb/ft^3)	water conditions (lb)	volume (ft^3)	Kaolite and water (lb)	Kaolite (lb)	water (lb)	Kaolite and water (lb)	Kaolite (lb)	water (lb)
97	87.5	393.5	356.5	197.0	22.29	306.00	4.91	269.00	107.60	161.40	109.50	107.60	1.90
98	87.5	393.5	356.5	198.5	22.60	306.00	4.91	269.00	107.60	161.40	111.00	107.60	3.40
54	87.5	395.0	356.5	199.0	22.59	307.50	4.94	269.00	107.60	161.40	111.50	107.60	3.90
87	87.5	394.0	353.5	196.5	22.16	306.50	4.92	266.00	106.40	159.60	109.00	106.40	2.60
2	88.0	394.0	360.0	202.5	23.31	306.00	4.91	272.00	108.80	163.20	114.50	108.80	5.70
4	88.0	395.5	360.0	203.0	23.30	307.50	4.94	272.00	108.80	163.20	115.00	108.80	6.20
42	88.0	394.5	356.5	199.5	22.66	306.50	4.92	268.50	107.40	161.10	111.50	107.40	4.10
43	88.0	396.0	357.5	198.0	22.25	308.00	4.94	269.50	107.80	161.70	110.00	107.80	2.20
94	87.0	393.5	361.5	205.0	23.98	306.50	4.92	274.50	109.80	164.70	118.00	109.80	8.20
35	88.0	394.5	363.5	208.0	24.39	306.50	4.92	275.50	110.20	165.30	120.00	110.20	9.80
3	87.0	393.0	364.0	206.0	24.23	306.00	4.91	277.00	110.80	166.20	119.00	110.80	8.20
44	88.0	394.0	356.5	204.5	23.72	306.00	4.91	268.50	107.40	161.10	116.50	107.40	9.10
32	88.0	396.0	355.0	198.5	22.35	308.00	4.94	267.00	106.80	160.20	110.50	106.80	3.70
33	87.5	394.0	351.0	197.5	22.36	306.50	4.92	263.50	105.40	158.10	110.00	105.40	4.60
58	87.5	394.5	351.5	196.5	22.12	307.00	4.93	264.00	105.60	158.40	109.00	105.60	3.40
4	87.5	394.0	343.0	192.5	21.34	306.50	4.92	255.50	102.20	153.30	105.00	102.20	2.80
22	87.5	394.5	352.0	196.0	22.02	307.00	4.93	264.50	105.80	158.70	108.50	105.80	2.70
27	88.0	395.5	352.5	196.5	21.98	307.50	4.94	264.50	105.80	158.70	108.50	105.80	2.70
28	87.5	394.5	350.5	199.0	22.63	307.00	4.93	263.00	105.20	157.80	111.50	105.20	6.30
30	87.5	395.0	352.0	200.0	22.79	307.50	4.94	264.50	105.80	158.70	112.50	105.80	6.70
27	88.0	395.5	352.5	196.5	21.98	307.50	4.94	264.50	105.80	158.70	108.50	105.80	2.70
mean	87.67	394.50	355.36	199.55	22.72	306.83	4.93	267.69	107.08	160.61	111.88	107.08	4.80
std. dev.					0.8132						100%	95.71%	4.29%
computed on means					22.72	306.83	4.93	267.69	107.08	160.61	111.88	107.08	4.80

Table 6.9.3.4-3. Fabrication data, before and after baking the top plug parts of the ES-2100 shipping package

								before baking			after baking		
Part Serial Number	clean & empty (lb)	filled with water (lb)	before baking (lb)	after baking (lb)	density after baking (lb/ft^3)	water conditions (lb)	volume (ft^3)	Kaolite and water (lb)	Kaolite (lb)	water (lb)	Kaolite and water (lb)	Kaolite (lb)	water (lb)
97	10.5	60.0	53.5	28.5	22.65	49.50	0.79	43.00	17.20	25.80	18.00	17.20	0.80
83	10.5	59.0	50.5	27.0	50.50	27.00	50.50	27.00	16.00	24.00	16.00	24.00	16.00
86	10.5	60.0	50.5	27.5	21.40	49.50	0.79	40.00	16.00	24.00	17.00	16.00	1.00
87	10.5	59.0	53.0	28.5	23.12	48.50	0.78	42.50	17.00	25.50	18.00	17.00	1.00
28	11.0	59.0	53.0	28.5	22.71	48.00	0.77	42.00	16.80	25.20	17.50	16.80	0.70
23	10.5	59.5	52.5	28.0	22.25	49.00	0.79	42.00	16.80	25.20	17.50	16.80	0.70
24	10.5	59.0	53.5	28.5	23.12	48.50	0.78	43.00	17.20	25.80	18.00	17.20	0.80
25	10.5	58.5	54.0	29.0	24.01	48.00	0.77	43.50	17.40	26.10	18.50	17.40	1.10
26	10.5	59.0	54.0	29.0	23.76	48.50	0.78	43.50	17.40	26.10	18.50	17.40	1.10
27	10.5	60.0	54.5	29.0	23.28	49.50	0.79	44.00	17.60	26.40	18.50	17.60	0.90
0	10.5	60.0	52.0	27.0	20.77	49.50	0.79	41.50	16.60	24.90	16.50	16.60	-0.10[a]
20	10.5	60.0	53.5	28.0	22.03	49.50	0.79	43.00	17.20	25.80	17.50	17.20	0.30
22	10.5	60.0	54.0	28.5	22.65	49.50	0.79	43.50	17.40	26.10	18.00	17.40	0.60
21	10.5	61.0	53.0	28.0	21.59	50.50	0.81	42.50	17.00	25.50	17.50	17.00	0.50
19	10.5	60.0	53.0	27.5	21.40	49.50	0.79	42.50	17.00	25.50	17.00	17.00	0.00
11	10.5	60.0	52.5	28.0	22.03	49.50	0.79	42.00	16.80	25.20	17.50	16.80	0.70
14	10.5	60.0	52.5	27.5	21.40	49.50	0.79	42.00	16.80	25.20	17.00	16.80	0.20
15	10.5	60.5	54.0	28.0	21.80	50.00	0.80	43.50	17.40	26.10	17.50	17.40	0.10
16	10.5	59.0	52.0	27.5	21.84	48.50	0.78	41.50	16.60	24.90	17.00	16.60	0.40
17	10.5	60.5	54.5	28.5	22.43	50.00	0.80	44.00	17.60	26.40	18.00	17.60	0.40
mean	10.52	59.70	53.00	28.10	23.74	48.10	3.28	42.48	16.99	25.48	17.58	16.99	0.58
std. dev.					6.3565						100%	96.67%	3.33%
computed on means					22.27	49.18	0.79	42.48	16.99	25.48	17.58	16.99	0.58

[a] No explanation is given for the negative amount of water in Part 0. Also, the smaller percentage of water present in the top plug compared with to the drum body weldment is attributed to the larger surface-to-volume ratio, which results in better drying of the parts.

The Kaolite components of ES-3100 shipping package had not been manufactured at the time this criticality safety evaluation was performed. Given the lack of production data for ES-3100 Kaolite, a material specification (mass and density) was derived from data for ES-2100 production units. This specification, denoted "as-manufactured" (AM) Kaolite, was used for the ES-3100 criticality calculations. This ES-2100 shipping package is similar in design to the ES-3100 currently being evaluated.

The Kaolite production process was re-evaluated and improved following the production of ES-3100 units. (Y/DW-1890) Test samples were produced. These were classified into three groups: high density, medium density, and low density. The predominate number of samples fell into the medium density category (22.04 lb/ft^3), representing the expected, improved Kaolite production process. (Y/DW-1890, Appendix 2.10.4, Table 5) A material specification for use in criticality calculations was derived from the medium density "test sample" (TS) Kaolite data. However, the TS data are based on small sample volumes, whereas the AM data represents the entire package. Taking into consideration both the potential for scaling error and the uncertainty of how representative the test samples are of the manufactured ES-2100 units, the criticality safety packaging analysts chose to utilize the material specification derived from AM data rather than TS data in the criticality calculations for the ES-3100 safety analysis report.

A set of criticality calculations was performed for each of the packaging material specifications (i.e., the TS and the AM Kaolite) using three package water contents to represent the range of NCT and HAC. Y-12 statisticians were asked to determine whether or not the observed differences in neutronic performance are statistically significant for a package modeled with the TS specification versus one modeled with the AM specification. The purpose of this discussion is to summarize this comparison (DAC-FS-900000-A014) and draw conclusions.

Criticality Calculations. Each case is rerun using a different starting random number in order to produce computed k_{eff} values that are statistically independent. Table 6.9.3.4-4 presents the random starting number, the mean value (k_{eff}) and corresponding standard error (s_i) computed for 10 individual runs of each case.

Three sets of criticality calculations were run for both the AM Kaolite and TS Kaolite. One set of calculaitons is for dry Kaolite (i.e., low water content, IS = 1e-04 sp gr water); another set is for normal moisture Kaolite (i.e., NCT water content); and the third set is for flooded Kaolite (i.e., high water content, IS = 1.0 sp gr water). These conditions span the range of NCT and HAC addressed in the criticality evaluation. An infinite array of packages was evaluated in order to eliminate any biases arising from spectral leakage effects in the reflector of the finite array. Each package was modeled having 36 kg of 100% enriched uranium in the form of 3.24-in. diameter cylinder content. The k_{eff} values for each KENO V.a case are based on 500,000 neutron histories produced by running for 215 generations with 2,500 neutrons per generation and truncating the first 15 generations of data.

Statistical evaluation. A review of KENO V.a calculation results was made to determine if a statistically significant difference exists between the mean k_{eff} for the TS Kaolite specification and the AM Kaolite material specifications used in the criticality evaluation of the ES-3100 shipping package. Case results were classified into three groups (i.e., low water content, medium water content, or high water content) depending on the amount of water present in the ES-3100 shipping package. The symbol "I" is used to specify the group. The mean difference and standard deviation for each of the three (3) sets of pair-wise differences was defined as follows:

(a) $d_i = (k_{effBi} - k_{effAi})/n$ and

(b) $s_{di} = \sqrt{[\, [\, n\Sigma d_i^{\,2} - (\, \Sigma d_i\,)^2\,]\,/\, n(n-1)\,]}$ (conservatively defined for the t-test appropriate for small sample sizes)

Table 6.9.3.4-4. Data for the statistical evaluation of "as-manufactured"and "test sample" Kaolite

As-Manufactured Kaolite				Test Sample Kaolite			
Case name	Random number	k_{eff}	s_i	Case name	Random number	k_{eff}	s_i
Group 1 – Low water content							
esrandnum_01_01_in	109E77866CF	1.00274	0.00138	mdrandnum_01_01_in	109E77866CF	1.00170	0.00125
esrandnum_01_02_in	16AA4A58735	1.00224	0.00120	mdrandnum_01_02_in	16AA4A58735	1.00416	0.00116
esrandnum_01_03_in	1814171B652	1.00121	0.00107	mdrandnum_01_03_in	1814171B652	1.00208	0.00125
esrandnum_01_04_in	1A423B9472C	1.00367	0.00118	mdrandnum_01_04_in	1A423B9472C	1.00271	0.00131
esrandnum_01_05_in	20E876D8224	1.00290	0.00133	mdrandnum_01_05_in	20E876D8224	1.00406	0.00125
esrandnum_01_06_in	3F6E65CA744	1.00266	0.00137	mdrandnum_01_06_in	3F6E65CA744	1.00418	0.00124
esrandnum_01_07_in	479D21DB750	1.00393	0.00108	mdrandnum_01_07_in	479D21DB750	1.00193	0.00133
esrandnum_01_08_in	55D4371D3A2	1.00313	0.00113	mdrandnum_01_08_in	55D4371D3A2	1.00196	0.00105
esrandnum_01_09_in	6E1A14672B8	1.00343	0.00119	mdrandnum_01_09_in	6E1A14672B8	1.00503	0.00118
esrandnum_01_10_in	77A0308C0E4	1.00229	0.00113	mdrandnum_01_10_in	77A0308C0E4	1.00358	0.00108
Group 2 – NCT medium density							
esrandnum_06_01_in	109E77866CF	0.99025	0.00119	mdrandnum_06_01_in	109E77866CF	0.98323	0.00118
esrandnum_06_02_in	16AA4A58735	0.98863	0.00128	mdrandnum_06_02_in	16AA4A58735	0.98630	0.00108
esrandnum_06_03_in	1814171B652	0.98811	0.00120	mdrandnum_06_03_in	1814171B652	0.98328	0.00125
esrandnum_06_04_in	1A423B9472C	0.98933	0.00114	mdrandnum_06_04_in	1A423B9472C	0.98487	0.00112
esrandnum_06_05_in	20E876D8224	0.98869	0.00103	mdrandnum_06_05_in	20E876D8224	0.98559	0.00109
esrandnum_06_06_in	3F6E65CA744	0.98854	0.00117	mdrandnum_06_06_in	3F6E65CA744	0.98412	0.00106
esrandnum_06_07_in	479D21DB750	0.98900	0.00119	mdrandnum_06_07_in	479D21DB750	0.98395	0.00118
esrandnum_06_08_in	55D4371D3A2	0.98844	0.00113	mdrandnum_06_08_in	55D4371D3A2	0.98546	0.00114
esrandnum_06_09_in	6E1A14672B8	0.99007	0.00126	mdrandnum_06_09_in	6E1A14672B8	0.98424	0.00121
esrandnum_06_10_in	77A0308C0E4	0.99028	0.00122	mdrandnum_06_10_in	77A0308C0E4	0.98465	0.00118
Group 3 – High water content							
esrandnum_09_01_in	109E77866CF	0.92872	0.00118	mdrandnum_09_01_in	109E77866CF	0.92800	0.00123
esrandnum_09_02_in	16AA4A58735	0.92800	0.00110	mdrandnum_09_02_in	16AA4A58735	0.92817	0.00107
esrandnum_09_03_in	1814171B652	0.92844	0.00118	mdrandnum_09_03_in	1814171B652	0.92770	0.00115
esrandnum_09_04_in	1A423B9472C	0.92780	0.00123	mdrandnum_09_04_in	1A423B9472C	0.92763	0.00126
esrandnum_09_05_in	20E876D8224	0.92783	0.00134	mdrandnum_09_05_in	20E876D8224	0.92584	0.00105
esrandnum_09_06_in	3F6E65CA744	0.92809	0.00128	mdrandnum_09_06_in	3F6E65CA744	0.92853	0.00112
esrandnum_09_07_in	479D21DB750	0.92725	0.00111	mdrandnum_09_07_in	479D21DB750	0.92682	0.00111
esrandnum_09_08_in	55D4371D3A2	0.92622	0.00126	mdrandnum_09_08_in	55D4371D3A2	0.92706	0.00116
esrandnum_09_09_in	6E1A14672B8	0.92925	0.00132	mdrandnum_09_09_in	6E1A14672B8	0.92733	0.00110
esrandnum_09_10_in	77A0308C0E4	0.92757	0.00114	mdrandnum_09_10_in	77A0308C0E4	0.92886	0.00132

where A_i denotes the TS by group classification, B_i the AM by group classification, and n the sample size of ten (10). It is reasonable to assume that the paired differences have been randomly selected from a normally distributed population of paired differences with mean μ_d and standard deviation σ_d. Therefore, the sampling distribution of

$$(d - \mu_d) / (s_d/\sqrt{n})$$

is a *t*-distribution having n-1 degrees of freedom.

The evaluation of the mean differences (d_i) for the 10 set of cases is accomplished through hypothesis testing, a statistical tool used to provide evidence that a difference exists or does not exist. The t_i values are 0.70, 10.0 and 0.95 for dry Kaolite, for NCT Kaolite, and for flooded Kaolite, respectively. A value of 3.25 is obtained from the standard table for critical values for the t distribution, from which the decision to accept or reject the null hypothesis H_0 is made with a Type I error probability (α) of 0.01. For $t < 3.25$, the H_0 hypothesis is not rejected. Acceptance of the null hypothesis is the result of insufficient evidence to reject it. Thus, it can be concluded that the mean estimate of the difference of the AM Kaolite is not significantly different from the mean of the TS Kaolite for both dry and flooded Kaolite. For $t > 3.25$, the H_0 hypothesis is rejected. Therefore, it can be concluded that the mean estimate of the difference of the AM Kaolite is significantly different from the mean of the TS Kaolite for the normal moisture Kaolite. The mean k_{eff} for AM Kaolite is significantly greater than the mean k_{eff} of the TS Kaolite; therefore, the use of the AM specification in the ES-3100 criticality calculations is conservative and bounding. Details of the statistical evaluation are documented in Reference DAC-FS-900000-A014.

6.9.3.5 WATER

Water is used in various regions of the models to simulate HAC as an interstitial moderator and as a reflector. When used at full density, the density of water is 0.9982 g/cm^3. (SCALE, Vol. 3, Sect. M8)

6.9.3.6 CALCULATION OF EQUIVALENT WATER MASS FOR POLYETHYLENE

In the calculation models for evaluation of NCT, water may be substituted for the polyethylene composition of bags present in the package. Based on hydrogen density, 1285.14 g of water are equivalent to 1000 g of polyethylene for nuclear criticality safety calculations. The equivalent water mass is calculated as follows:

Hydrogen in 1 kg of polyethylene [$(CH_2)_2$, molecular weight = 28.0312; density = 0.92]:

$$\text{1 kg polyethylene} = \frac{1000\ \text{g}}{0.92\ \text{g/cm}^3} = 1087.0197\ \text{cm}^3$$

$$\text{H number density} = \frac{(0.92)(4)(6.02252\times10^{23})}{(28.0312)(10^{24})} = 7.906502\times10^{-2}\ \text{at/bn-cm}$$

$$\text{H in 1 kg} = (1087.0197\text{cm}^3)(7.906502\times10^{-2}) = 85.945234\ \text{at-cm}^2\text{/bn}$$

Grams of water [H_2O, molecular weight = 18.0110; density = 0.9982] with hydrogen content equivalent to 1 kg of polyethylene:

$$\text{equivalent g of } H_2O = \frac{(85.945234)(18.0110)(10^{24})}{(2)(6.02252\times10^{23})} = 1285.1427\ \text{g}$$

Appendix 6.9.4

QUALIFICATION OF A NEUTRON ABSORBER MATERIAL FOR THE ES-3100

Appendix 6.9.4

QUALIFICATION OF A NEUTRON ABSORBER MATERIAL FOR THE ES-3100

6.9.4.1 INTRODUCTION

277-4 is a formulation of Thermo Electron Corporation's Cat. 277-0, a boron carbide additive and water. 277-4 is a neutron radiation shielding product and is one of several materials in its class that have been evaluated as a candidate neutron absorber system for a variety of nuclear criticality safety applications by the Y-12 National Security Complex (Y-12). This class of materials is characterized as a dispersion of $^{nat}B_4C$ particulate* throughout a hardened hydraulic cement or binder, resulting in a high-hydrogen, borated material system. It offers many advantages for typical Y-12 applications over other classes of materials such as borated aluminum because a neutron moderator and neutron absorber are both integral to the solid material system itself. The separate addition of another neutron moderating material such as water or polyethylene is not required in order for it to function effectively.

Computational methods of analysis in simple geometry permit direct comparison of neutron absorber system performance for nuclear criticality safety applications. The measure of comparison is the neutron interaction potential between two parallel 0.745-cm-thick slabs of infinite extent of ^{235}U metal at a density of 18.81 g/cm^3. The slabs are separated by a variable thickness of material and reflected by a 60-cm thickness of the same material (Fig. 6.9.4.1-1). Each material is modeled as an idealized homogenous mixture of elements based on nominal density and constituent proportions (Table 6.9.4.1-1). The result is expressed in terms of calculated k_{eff}† as influenced by the thickness of the candidate material between the two parallel slabs (see Fig. 6.9.4.1-2).

The least effective neutron absorber material systems are those with low hydrogen content and low neutron absorption cross section (e.g., ordinary concrete). The performance of concrete that contains $^{nat}B_4C$ particulate (e.g., borated concrete) is improved, but it is still hindered by its low hydrogen content. This is a function of the proportion and type of cement in the typical concrete mixture (i.e., a low proportion of lime- and silica-based Portland cement). Ordinary water is also included for comparison because of its high hydrogen content, but its performance is also limited by a low total mass density and low neutron absorption cross section.

As expected, materials with high hydrogen content and high boron content (e.g., 277-4, borated ceramics, and borated polymers) are predicted to be the most effective neutron absorber systems. Although the mechanical and thermal properties of such systems can vary significantly, their nuclear properties are dictated almost exclusively by the relative proportion and content of ^{10}B and H and the total mass density of the material system. These things being equal, the nuclear performance of any material in this class (i.e., 277-4, borated ceramics, and borated polymers) is representative of the others.

---

*277-4 is an improved variant of the Cat 277 product ca. 2000 which was originally formulated as a dispersion of ^{nat}Borosilicate glass granules rather than the current practice of using $^{nat}B_4C$ particulate.

†SCALE 4.4a, CSAS25 code sequence for KENO V.a with the 238-group ENDF B-IV neutron cross-section library on the Y-12 SAE Hewlett-Packard J5600 workstation (CMODB).

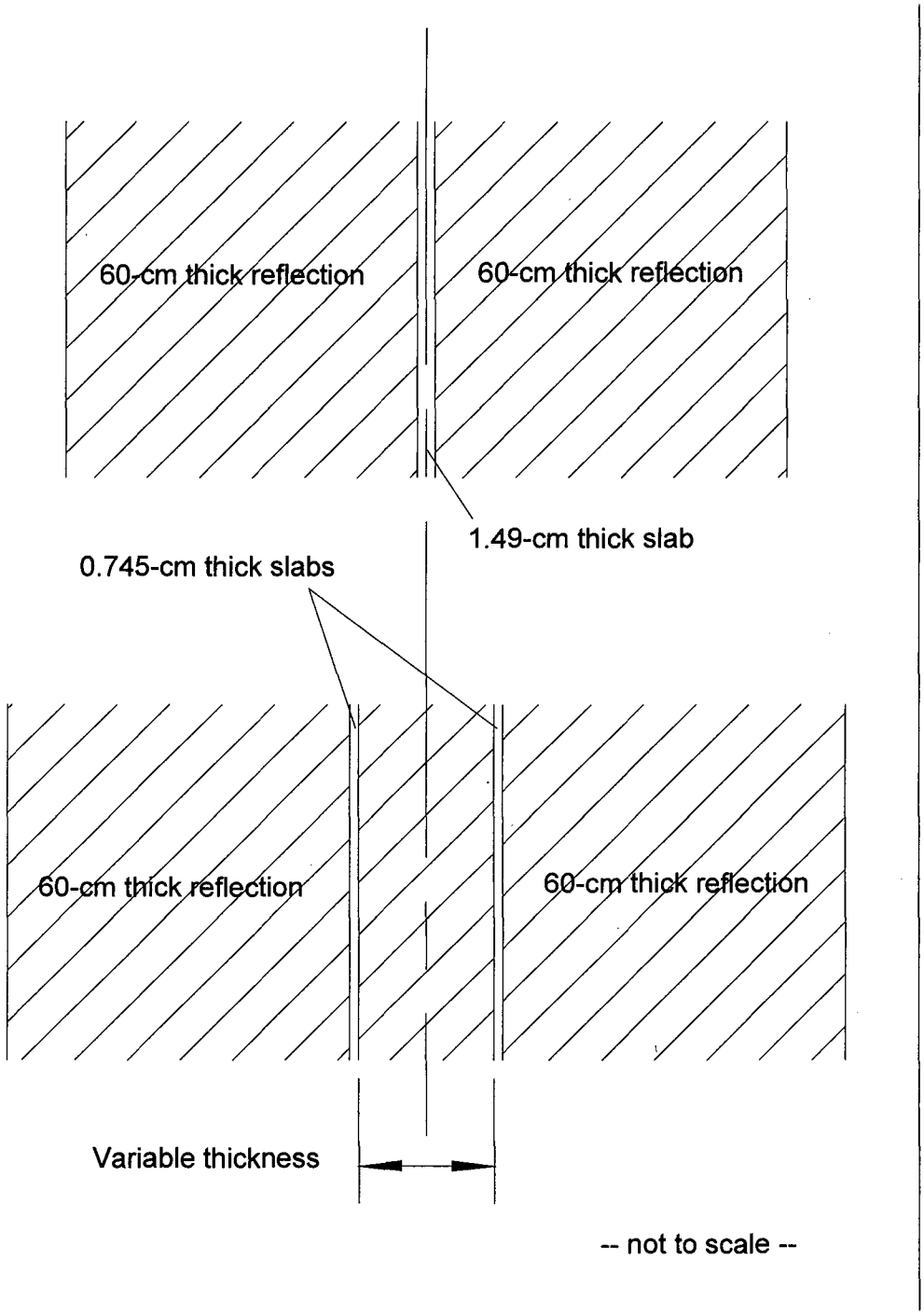

Fig. 6.9.4.1-1. Physical model of parallel ^{235}U metal slabs of infinite extent reflected and separated by various candidate neutron absorber materials.

Table 6.9.4.1-1. Nominal elemental and isotopic compositions of idealized material models for comparison of various neutron absorbers (atoms/barn·cm)

	Ordinary Concrete A 2.147 g/cm³	Ordinary Concrete B 2.299 g/cm³	Water 0.9982 g/cm³	Borated Concrete 2.563 g/cm³	Cat 277[a] 1.68 g/cm³	Borated Ceramic 1.91 g/cm³	Borated Polymer 1.717 g/cm³	^{235}U Metal 18.81 g/cm³
H	4.2581e-03	8.5010e-03	6.6751e-02	4.2900e-03	3.3800e-02	2.7200e-02	5.7600e-02	
B-10				1.7600e-04	2.8400e-04	2.6500e-03	9.4600e-04	
B-11				6.8100e-04	1.1800e-03	1.1000e-02	3.9200e-03	
C	1.1348e-02	2.0217e-02		9.0000e-04		4.2600e-03	2.3500e-02	
N							1.3800e-03	
O	4.0370e-02	3.5511e-02	3.3376e-02	4.2400e-02	3.7100e-02	3.2900e-02	2.5900e-02	
Na	7.9356e-05	1.6299e-05		6.7100e-05	2.6000e-04	7.9200e-05		
Mg	5.0111e-03	1.8602e-03		2.3000e-04	2.0800e-04	2.3300e-03		
Al	3.7660e-04	5.5580e-04		2.2900e-03	8.9700e-03	1.7400e-03	7.7000e-03	
Si	1.9382e-03	1.7000e-03		1.1800e-02	7.6700e-04	3.2300e-03		
P						2.1200e-03		
S	1.0013e-04			9.6300e-05	6.0000e-05	7.7800e-05		
Cl	1.9074e-05							
K	3.1231e-04	4.0300e-05		3.1600e-04		2.3100e-03		
Ca	7.3008e-03	1.1101e-02		3.1200e-03	2.2300e-03	2.4600e-04		
Ti	4.0183e-05					7.0800e-05		
Mn	1.2050e-05			1.4000e-04				
Fe	1.2954e-04	1.9301e-04		4.6200e-03	4.8900e-05	5.2000e-04		
U-235								4.8200e-02

[a] The ^{10}B content of this material model for Cat 277 is based on its ca. 2000 formulation using crushed borosilicate glass rather than the current practice of using $^{nat}B_4C$ particulate. This particular formulation is roughly equivalent to ~2% $^{nat}B_4C$ particulate (i.e., equivalent ^{10}B content, by weight). For otherwise identical H and B-10 content, this difference is unimportant relative to its nuclear performance as an idealized homogeneous mixture of elements. However, the current use of more than 5% $^{nat}B_4C$ particulate (by weight) is preferred due to reasons relating to the method of preparation, chemical reaction, and placement of 277-4 and uniformity of ^{10}B distribution in the cured product. As with all the materials in this class, the amount of H and ^{10}B in the finished product is determined by the relative proportions of its major constituents, which are tailored to the requirements of the specific application.

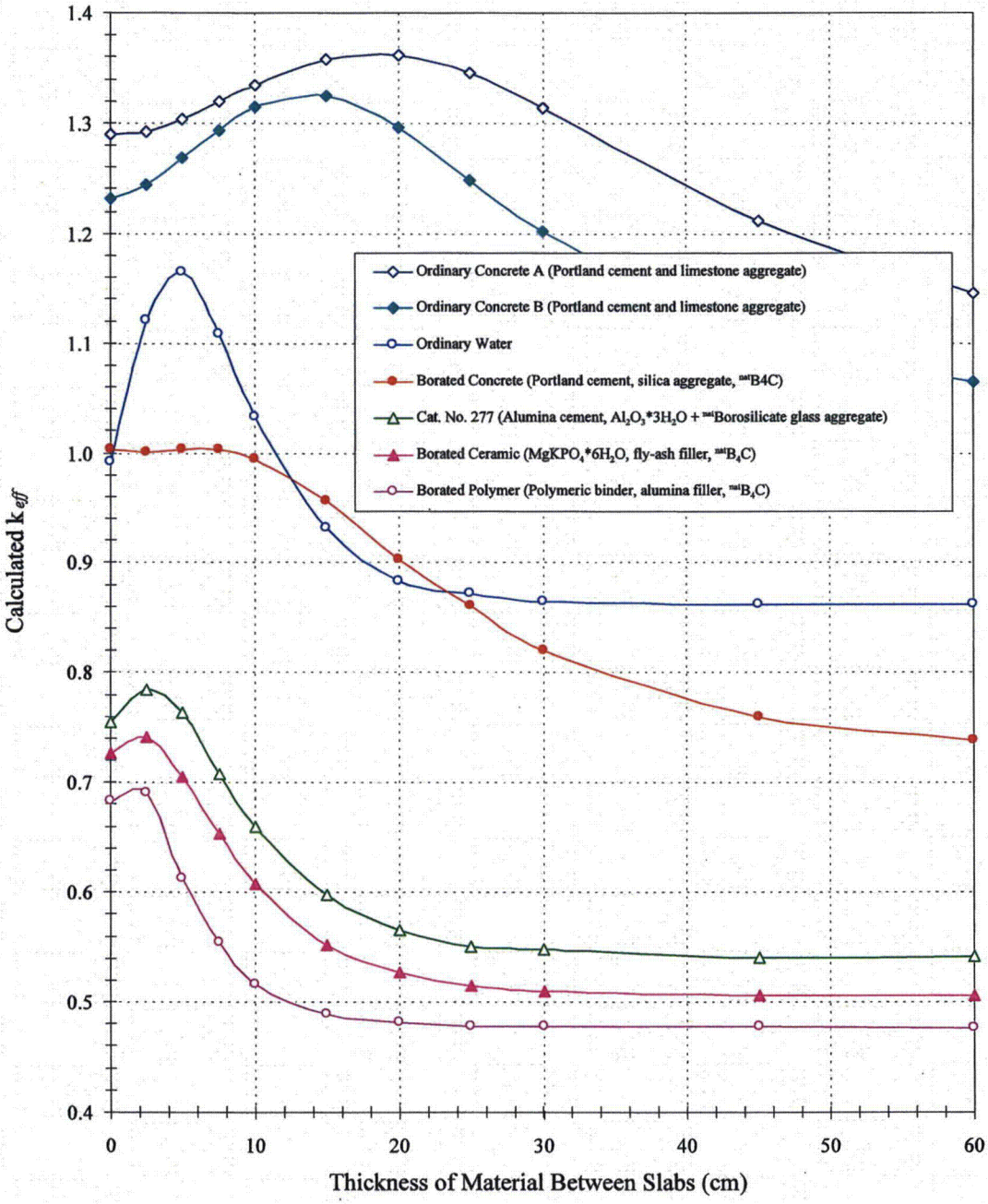

Fig. 6.9.4.1-2. The effect of various materials on neutron interaction between parallel slabs of ^{235}U metal of infinite extent.

6.9.4.2 PERFORMANCE TESTING

To investigate the performance of this class of neutron absorbing materials further, Y-12 has studied neutron radiography and neutron transmission measurements on several samples of a borated ceramic. Like 277-4, the borated ceramic is also a dispersion of $^{nat}B_4C$ particulate throughout a hardened hydraulic crystalline solid material matrix for which the binder phase is $MgKPO_4 \cdot 6H_2O$ rather than the hydrates of CaO and Al_2O_3. In fact, the more finely divided $^{nat}B_4C$ particulate specified for 277-4 is a slight advantage over the modestly coarser particulate in the borated ceramic. As shown below in Table 6.9.4.2-1, the relative proportion and content of H and ^{10}B and their total mass density are very similar. The small differences between the nuclear properties of their associated low- and intermediate-Z elements (i.e., oxides of Mg, Al, P, K, and Ca) are negligible. Thus, performance and the most significant factors affecting performance are nearly identical for both materials, so the results of neutron radiography and neutron transmission for the borated ceramic samples are judged applicable to 277-4 specimens of similar dimension.

Table 6.9.4.2-1. Comparison of nominal values for 277-4 and borated ceramic samples subjected to neutron radiography and neutron transmission testing.

Attribute	Cat 277 Original Formulation ca. 2000	277-4 ES-3100 Formulation as Cured	Borated Ceramic Samples for Testing
Principal Binder Phase(s)	Hydrates of CaO and Al_2O_3	Hydrates of CaO and Al_2O_3	$MgKPO_4 \cdot 6H_2O$
Neutron Absorber Particle Size	^{nat}Borosilicate glass granules 90 wt % <2360 μm 65 wt % <1180 μm 40 wt % <600 μm 15 wt % <102 μm 0 wt % <150 μm	$^{nat}B_4C$ particulate 100 wt % <102 μm	$^{nat}B_4C$ particulate 100 wt % <559 μm 90 wt % <356 μm 40 wt % <254 μm 3 wt % <122 μm 0 wt % <63 μm
Filler Material(s)	$Al_2O_3 \cdot 3H_2O$	$Al_2O_3 \cdot 3H_2O$	Class F Coal Fly-ash
Total Mass Density	1.68 g/cm^3	1.60 g/cm^3	1.91 g/cm^3
Total H_2O content	0.51 g/cm^3	0.51 g/cm^3	0.49 g/cm^3
Total ^{10}B content	0.005 g/cm^3	0.013 g/cm^3	0.012 g/cm^3

Samples were prepared from sectioned pieces of a single specimen from a vertically oriented mold measuring 10 × 10 × ~30 cm tall, as illustrated in Fig. 6.9.4.2-1 (nominally 4 × 4 × 12 in. tall). One specimen was prepared by the normal method of mixing and preparation for the borated ceramic material. Sectioning the first specimen resulted in two thick samples designated "1 of 2" and "2 of 2" which each measured 10-cm wide by ~30-cm long by ~2.4-cm thick (nominally 1-in. thick). A second specimen was prepared by abnormal methods intended to produce non-homogeneity (i.e., poorly mixed using retardants followed by excessive and extended vibration of the mold after installation). Sectioning this specimen resulted in two thin samples designated "062d1bc" and "062d1bd" which each measured 10-cm wide by ~30-cm long by ~1.2-cm thick (nominally 0.5-in. thick). The samples were delivered to the Breazeale Nuclear Reactor Building at Pennsylvania State University for inspection. Upon completion of inspection for all four samples as received, a thick sample "1 of 2" and a thin sample "062d1bc" were dehydrated by heating to 140°C to eliminate interference by hydrogen, and all four samples were tested again.

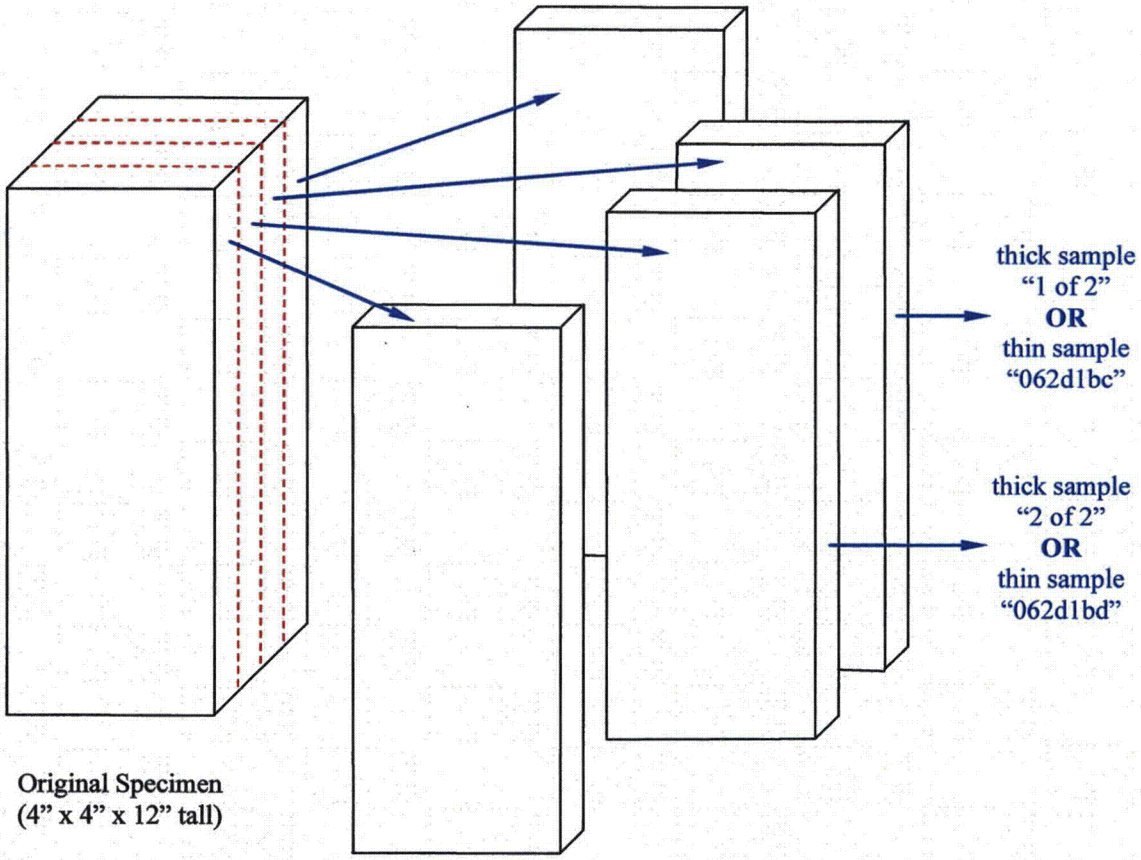

Fig. 6.9.4.2-1. Illustration of sectioning plan for borated ceramic samples for neutron radiography and neutron transmission measurements.

All four samples were qualitatively inspected for visual defects and subjected to neutron radiographic inspection. The inspections were intended to identify any variations in image luminance, which would indicate a variation in homogeneity and density. Neutron transmission measurements were calibrated to results for thin ZrB_2 reference coupons sandwiched with thick aluminum metal. The ^{10}B areal densities of the thin reference coupons ranged from 5.32 mg/cm^2 to 57.04 mg/cm^2 over a total ZrB_2 + Al reference thickness of 24.21–24.98 mm. By comparison, the thick samples contain an idealized ^{10}B areal density of 28.8 mg/cm^2 (i.e., 0.012 g/cm^3 over a 2.4-cm thickness), and the thin samples contain an idealized ^{10}B areal density of 14.4 mg/cm^2 (i.e., 0.012 g/cm^3 over a 1.2-cm thickness).

Radiographic examination of both thick samples "1 of 2" and "2 of 2" indicated uniformity of composition and density (see Fig. 6.9.4.2-2). Even after dehydration of thick sample "1 of 2," radioscopic examination indicated uniformity of composition and density. Initial neutron transmission results for both thick samples "1 of 2" and "2 of 2" indicated that neutron transmission was very low. In fact, the interference due to the hydrogen content implies an equivalent ^{10}B areal density measurement of ~67 ± 4 mg/cm^2. This is more than twice the actual physical value of 28.8 mg/cm^2. Only after thick sample of "1 of 2" is dehydrated and tested again do the results of neutron transmission measurements more accurately reflect the actual physical ^{10}B content. In fact, the average measured value of 27.419 mg/cm^2 at eleven points along the long axis of the dehydrated sample "1 of 2" is more than 95% of the actual physical value of 28.8 mg/cm^2 and varies no more than a few percent from one end to the other (see Tables 6.9.4.2-2 and 6.9.4.2-3).

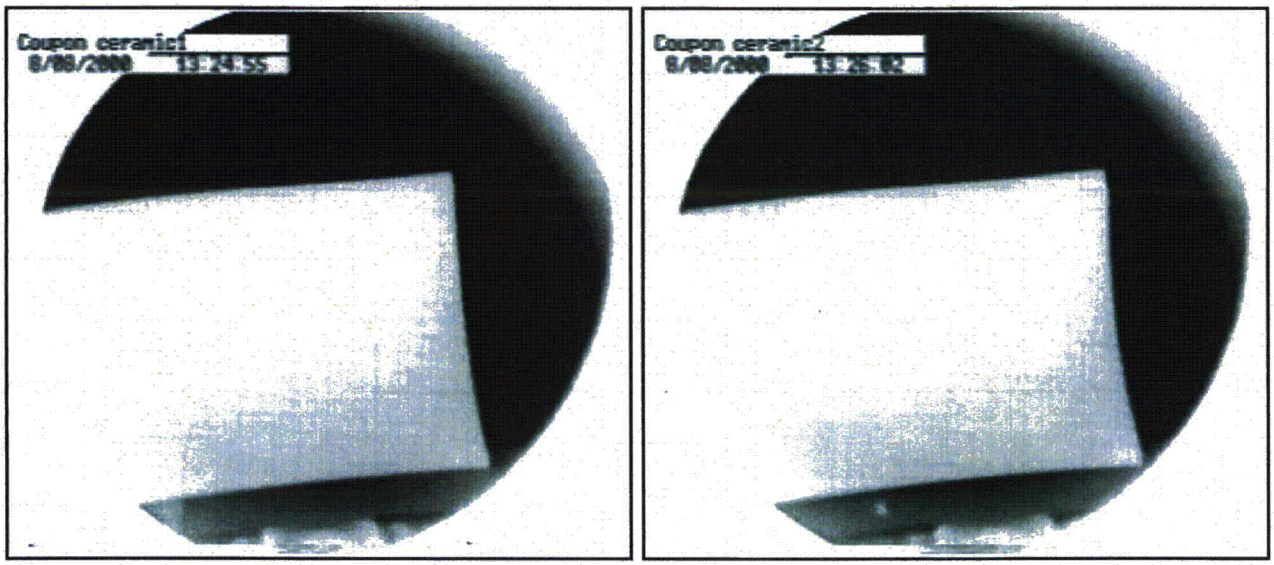

Fig. 6.9.4.2-2. Radiographic images of thick samples "1 of 2" (left) and "2 of 2" (right) indicating uniformity of composition and density.

Table 6.9.4.2-2. Results of neutron transmission measurements of thick samples

	Equivalent ^{10}B Areal Density (mg/cm^2)		
	End	**Center**	**End**
sample "1 of 2"	66.419	68.673	71.003
sample "2 of 2"	65.0	68.25	69.708
sample "1 of 2" (dehydrated)	27.586	27.191	28.555
sample "2 of 2" (re-test)	63.687	65.966	65.572

Table 6.9.4.2-3. Neutron transmission measurements of thick sample "1 of 2" after dehydration

Point of Measurement (uniform intervals from one end to the other)	Equivalent ^{10}B Areal Density (mg/cm^2)	Deviation from Average (%)
1	27.586	+0.6 %
2	26.909	-1.9 %
3	27.039	-1.4 %
4	27.358	-0.2 %
5	27.286	-0.5 %
6	27.191	-0.8 %
7	27.375	-0.2 %
8	27.179	-0.8 %
9	27.236	-0.7 %
10	27.897	-0.9 %
11	28.555	+4.1 %
Average	**27.419**	

Radiographic examination of both thin samples "062d1bc" and "062d1bd" indicates areas of nonuniformity and spots of lower neutron attenuation, along with greater dissimilarity between the samples themselves (see Fig. 6.9.4.2-3). Many of these areas and spots remained evident by radiographic examination even after dehydration of thin sample "062d1bc" and are attributed to physical voids revealed during visual inspection. Again, initial neutron transmission measurements implied a greater-than-actual equivalent ^{10}B areal density due to the interference of hydrogen (i.e., measured values averaged ~23.3 mg $^{10}B/cm^2$ rather than the actual value of 14.4 mg $^{10}B/cm^2$).

Measurements repeated after dehydration of sample "062d1bc" more correctly estimate the equivalent ^{10}B areal density to be ~11.1 mg/cm^2, which is ~77% of the actual physical ^{10}B content. Again, the relative values vary only a few percent from one end of the sample to the other (see Table 6.9.4.2-4). However, the measured values of a dehydrated sample in this case are known to be biased low. First, the total thicknesses of the ZrB_2 + Al reference coupons for calibration were ~24.21 to 24.98-mm compared to the 1.2-cm thickness of "062d1bc." Second, the total mass density of the sample is ~1.4 to 1.5 g/cm^3 after dehydration compared to an Al mass density of ~2.7 g/cm^3 for the ZrB_2 + Al reference coupons. This indicates that even the performance of the thin samples (i.e., 1.2-cm thickness) exhibiting non-uniformity of composition and density is only marginally reduced from that of the idealized, homogenous material model with respect to neutron absorber efficiency.

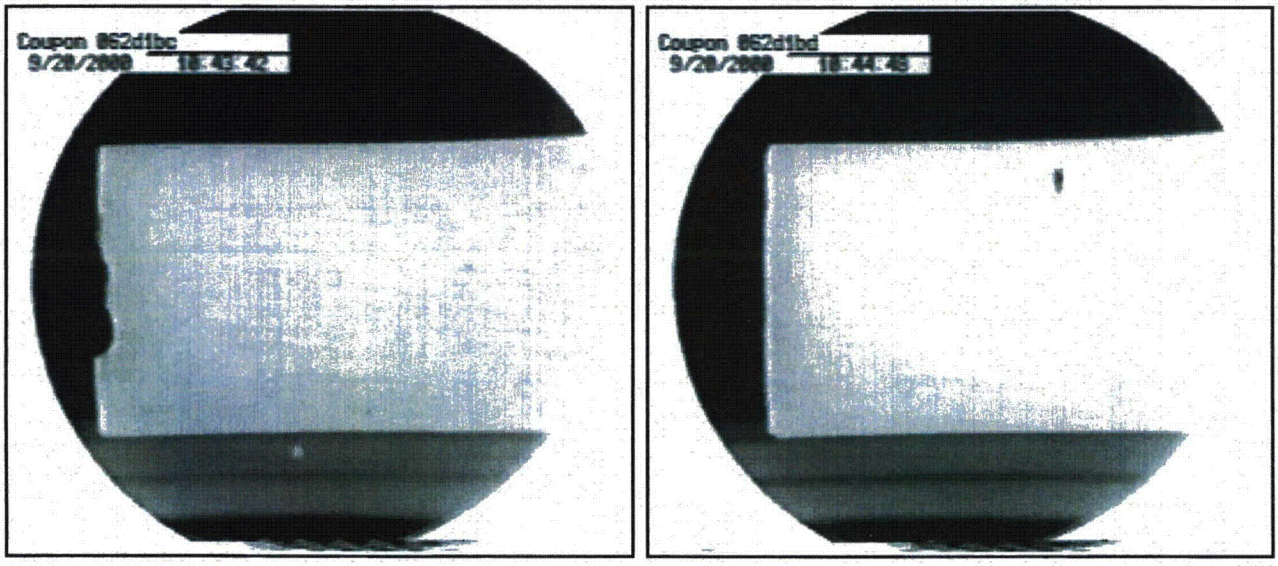

Fig. 6.9.4.2-3. Radiographic images of thin samples "062d1bc" (left) and "062d1bd" (right) indicating non-uniformity of composition and density and dissimilarity of samples.

Table 6.9.4.2-4. Neutron transmission results for dehydrated thin sample "062d1bc" and re-test of thin sample "062d1bd"

Position of Measurement (see Fig. 6.9.4.2-4)	Minimum Equivalent ^{10}B Areal Density (mg/cm^2)			
	Dehydrated Thin Sample "062d1bc"		Re-Test of Thin Sample "062d1bd"	
	Line A	Line B	Line A	Line B
1	12.227	11.781	25.909	25.154
2	11.776	11.462	24.390	25.344
3	11.388	11.252	24.257	24.645
4	10.554	10.462	25.341	24.885
5	10.432	10.528	24.646	25.483
6	10.754	11.728	25.450	25.712
7	10.396	11.534	25.761	23.063
8	11.166	10.221	24.522	25.257
9	10.875	10.459	23.113	23.882
10	11.051	10.676	25.270	23.724
11	11.258	11.214	24.922	25.355
Combined Average	11.1		24.8	

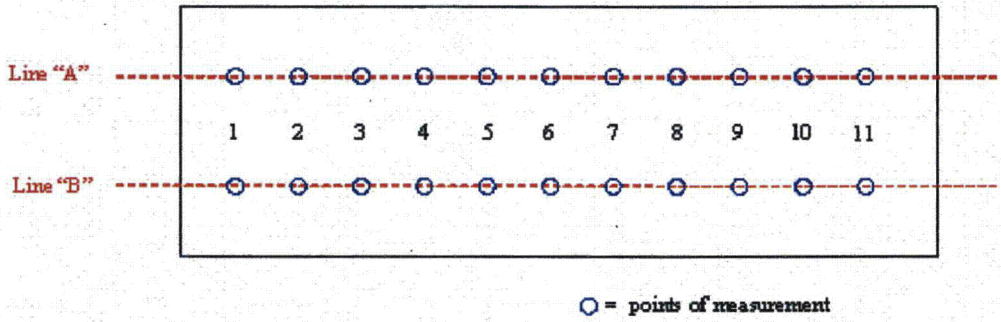

Fig. 6.9.4-6. Illustration of measurement plan for neutron transmission measurements of thin samples "062d1bc" and "062d1bd."

6.9.4.2.3 CONCLUSIONS

Provided that 277-4 is prepared in a controlled manner to ensure the proper specification and proportioning of batch constituents, thorough mixing of the wet slurry, and correct placement and installation to prevent large physical voids, a credible technical justification exists to credit no less than 75% f the $^{nat}B_4C$ particulate and its other constituents, by weight, as an idealized homogenous mixture for nuclear criticality safety analysis of the ES-3100. There is no evidence of non-homogeneity, neutron self-shielding effects, or neutron streaming effects in borated hydraulic cement or ceramic material systems for thicknesses of 2.4-cm or more. The qualification of 277-4 for use in the design and construction of the ES-3100 described herein is based on sound nuclear engineering principles and direct application of performance test results for such material systems.

Appendix 6.9.5

MISCELLANEOUS INFORMATION AND DATA

Appendix 6.9.5

MISCELLANEOUS INFORMATION AND DATA

Table 6.9.5.1 provides the atomic weights of the elements and isotopes of the materials used in this criticality safety evaluation. Atomic weights and isotopic weight percents of the naturally occurring materials are those taken from the Materials Information Processor in the SCALE Standard Composition Library.

Table 6.9.5.2 provides the molecular weights and weight percents of the corresponding elements and isotopes of the various compounds. The weight percents shown in this table are the input to KENO V.a. (SCALE, Vol. 2, Sect. F11)

Table 6.9.5.3 provides equations for determining atomic densities. These equations were derived based on the assumption that all constituents in the mixture are volume additive. Although these equations with their corresponding subscripts are for mixtures of elements, isotopes, or both, all except Equation (2) can be applied to compounds if the user substitutes certain subscript notations and meaning changes. For example, in Equations (1a) and (1b), the atomic weight becomes the molecular weight and the subscript "m" for mixture changes to the subscript "c" for compound. Likewise, in Equations (3a) and (3b), the atomic weight becomes the molecular weight, and the atom fraction (n_i) becomes the stoichiometric proportion of the elements making up the molecule. In Equations (3)–(5), the atom fraction (n_i) becomes the stoichiometric proportion (the element number subscript in the molecular formula), whose sum does not equal unity. Equation (2) is applicable only to the theoretical density of mixtures; it does not apply to the density of compounds.

Table 6.9.5.1. Atomic weights

Element or isotope	Atomic weight
H	1.0078
C	12.0000
O	15.9954
N	14.0033
Na	22.9895
Mg	24.3051
Al	26.9818
Si	28.0853
Ca	40.0803
Ti	47.8789
Cr	51.9957
Mn	54.9380
Fe	55.8447
Ni	58.6868
Zr	91.2196
^{235}U	235.0442
^{238}U	238.0510

Table 6.9.5.2. Molecular weights

Compound	Molecular or atomic weight	Weight percent in compound	Stoichiometric composition
Kaolite 1600™			
Alumina	-	9.6	Al_2O_3
Al	26.9818	52.92507	
O	15.9954	47.07493	
Silica	-	36.7	SiO_2
Si	28.0853	46.74349	
O	15.9954	53.25651	
Ferric Oxide	-	6.7	Fe_2O_3
Fe	55.8447	69.94330	
O	15.9954	30.05670	
Titanium Oxide	-	1.2	TiO_2
Ti	47.8789	59.95084	
O	15.9954	40.04916	
Calcium Oxide	-	30.7	CaO
Ca	40.0803	71.47009	
O	15.9954	28.52991	
Magnesium Oxide	-	13.1	MgO
Mg	24.3051	60.30359	
O	15.9954	39.69641	
Alkalies	-	2.0	Na_2O
Na	22.9895	74.18575	
O	15.9954	25.81425	

Table 6.9.5.3. Useful equations

N_m	=	$\rho_m N_o / A_m$.	(1a)
N_i	=	$w_i \rho_m N_o / A_i$.	(1b)
ρ_m	=	$1/\Sigma w_i/\rho_i$.	(2)
A_m	=	$1/\Sigma w_i/A_i$.	(3a)
	=	$\Sigma n_i A_i$	(3b)
w_i	=	m_i/m_m .	(4a)
	=	$n_i A_i / \Sigma n_i A_i$.	(4b)
n_i	=	N_i/N_m .	(5a)
	=	$(w_i/A_i)/\Sigma(w_i/A_i)$.	(5b)

where

N_o	=	0.602252×10^{24} (atoms/mole) Avogadro's number,
N	=	atom density (atoms/cm^3), $N_m = \Sigma N_i$,
ρ	=	density (g/cm^3) ,
A	=	atomic mass (g-mole) ,
w	=	weight fraction, $\Sigma w_i = 1$,
n	=	atom fraction, $\Sigma n_i = 1$,
subscript "m"	=	of the mixture ,
subscript "i"	=	i^{th} component of the mixture ,
(atoms/cm^3)(1/10^{24})	=	atoms/barn-cm.

Appendix 6.9.6

ABRIDGED SUMMARY TABLES OF CRITICALITY CALCULATION RESULTS